JCTC Journal of Chemical Theory and Computation

pubs.acs.org/JCTC Article

Performance of Density Functionals for Excited-State Properties of Isolated Chromophores and Exciplexes: Emission Spectra, Solvatochromic Shifts, and Charge-Transfer Character

Abhilash Patra,[§] George Baffour Pipim,[§] Anna I. Krylov,* and Shaama Mallikarjun Sharada*

Cite This: J. Chem. Theory Comput. 2024, 20, 2520−2537 Read Online

ACCESS | Metrics & More | Article Recommendations | Supporting Information

ABSTRACT: This study assesses the performance of various meta-generalized gradient approximation (meta-GGA), global hybrid, and range-separated hybrid (RSH) density functionals in capturing the excited-state properties of organic chromophores and their excited-state complexes (exciplexes). Motivated by their uses in solar energy harvesting and photoredox CO_2 reduction, we use oligo-(p-phenylenes) and their excited-state complexes with triethylamine as model systems. We focus on the fluorescence properties of these systems, specifically emission energies. We also consider solvatochromic shifts and wave function characteristics. The latter is described by using reduced quantities such as natural transition orbitals (NTOs) and exciton descriptors. The functionals are benchmarked against the experimental fluorescence spectra and the equation-of-motion coupled-cluster method with single and double excitations. Both in isolated chromophores and in exciplexes, meta-GGA functionals drastically underestimate the emission energies and exhibit significant exciton delocalization and anticorrelation between electron and hole motion. The performance of global hybrid functionals is strongly dependent on the percentage of exact exchange. Our study identifies RSH GGAs as the best-performing functionals, with ωPBE demonstrating the best agreement with experimental results. RSH meta-GGAs often overestimate emission energies in exciplexes and yield larger hole NTOs. Their performance can be improved by optimally tuning the range-separation parameter.

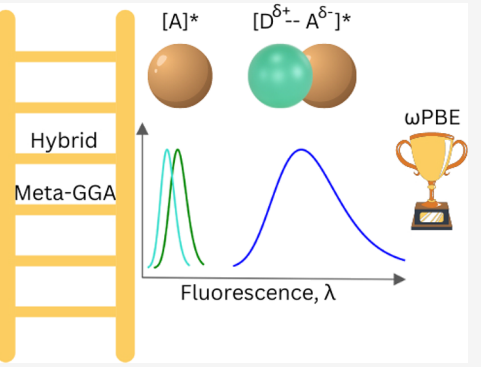

INTRODUCTION

Kohn−Sham density functional theory (KS-DFT)[1,2] and its time-dependent extension to excited states [TDDFT or linear-response TDDFT (LR-TDDFT)][3,4] are widely used to simulate the electronic structure of molecules, their aggregates, and materials.[5] The performance of both KS-DFT and LR-TDDFT depends critically on the exchange-correlation functional whose exact form is unknown.[5−7] Different strategies have been used to derive approximate functionals,[7] incorporating exact constraints and/or empirical expressions.[5] In general, a particular density functional approximation or class of functionals is better suited to predict specific sets of properties than others, assessed via careful benchmarking of functional performance to either experiments or high-level quantum chemical calculations.

In the context of excited-state calculations, significant efforts have been devoted to benchmarking functional performance in computing vertical excitation energies, absorption spectra, and Stokes shifts across a range of molecules and clusters.[8−17] Benchmarking emission spectra can be challenging as it necessitates computationally intensive calculations of optimization and verification of minima on excited-state potential energy surfaces as well as the availability of reliable reference data. As a result, most studies have been limited to examining functional performance on data sets consisting of relatively small molecules.[18] In benchmarking functional performance for excited states, it is important to go beyond excitation/emission energies and evaluate properties of the underlying wave functions — such as charge distributions in the excited states. These properties are important because they ultimately determine spectroscopic observables such as oscillator strengths and solvatochromic shifts.[19]

In this work, we carry out functional benchmarking of emission energies and wave function analysis of locally excited chromophores as well as charge-transfer (CT) complexes. Our choice of model systems is inspired by experimental studies which demonstrated that CO_2 can be effectively photoreduced in the presence of organic chromophores known as oligo-p-phenylenes (OPP-*N*, where *N* is the number of phenyl groups) to produce a range of products including formate, amino acids, and hydrocarboxylated styrenes.[20−22] The proposed catalytic cycle for single-electron reduction of CO_2 is initiated by

Received: January 3, 2024
Revised: February 26, 2024
Accepted: February 28, 2024
Published: March 15, 2024

https://doi.org/10.1021/acs.jctc.4c00005
J. Chem. Theory Comput. 2024, 20, 2520−2537

photoexcitation of OPP-*N*, followed by reductive quenching by a sacrificial donor (such as triethylamine, TEA) to generate a radical OPP-*N* anion that subsequently reduces CO_2 via electron transfer, regenerating OPP-*N* in the process. Two oligomers, *p*-terphenyl (OPP-3) and *p*-quaterphenyl (OPP-4), were found to be more viable owing to poorer solubility of longer chain oligomers.[20]

As reported by Kron et al.,[23] the experimental fluorescence spectra of OPP-3 in the presence of varying concentrations of TEA feature distinct emission peaks, corresponding to isolated [OPP-3]*, and red-shifted broad bands, characteristic of excited-state partial CT complexes, also known as exciplexes ([OPP-3−TEA]*). The likelihood of exciplex formation decreases with an increasing solvent dielectric constant. Formation of exciplexes is undesirable for CO_2 reduction as they are believed to decay back to the neutral ground-state species instead of completing electron transfer to [OPP-*N*]* to generate the quenched anion radical.

In this work, we evaluate the performance of different density functionals in computing the emission energies of isolated [OPP-*N*]* and their exciplexes, [OPP-*N*−TEA]*, (N = 3, 4). We benchmarked the computed emission energies against the experimental spectra. We benchmark the computed exciton properties of [OPP-*N*]* against equation-of-motion coupled-cluster calculations with single and double excitations (EOM-CCSD).[24,25]

The emission of the isolated chromophores, either in the gas phase or in solutions, is computed as a vertical transition at the optimized excited-state structure. This approach needs to be modified for describing exciplexes, which have more than one (closely spaced) minimum on the excited-state potential energy surface. In a recent publication, we introduced a systematic approach for computing the emission spectra of exciplexes.[26] Our protocol entails generating and verifying an ensemble of geometries to represent the exciplex state. The emission spectrum is calculated by summing over emission from all of the structures constituting the ensemble weighted according their Boltzmann populations. The exciplexes show significant CT character, which we use to distinguish exciplexes from other excited-state minima. We quantify electronic properties using natural transition orbitals (NTOs), wave function analysis tools, and exciton descriptors.[19,27−37] Specifically, we consider the vectorial electron−hole distance ($d_{h\rightarrow e}$), electron size (σ_e), hole size (σ_h), exciton size (d_{exc}), and electron−hole correlation (R_{eh}). These descriptors facilitate comparisons between different functionals as well as against many-body treatments, such as EOM-CCSD. They also provide a deeper insight into the performance of the functionals in the challenging case of states with significant CT character.

Calculations of the emission spectra of exciplexes are more onerous than calculations of the emission of isolated chromophores because the exciplex state is defined by a distribution or ensemble of structures. The quality of the resulting spectra depends on multiple factors, including the choice of density functional and a basis set, the solvent model,[38,39] as well as the quality of the computed geometries. Importantly, the computational method should be able to describe both locally excited states and the states involving significant CT character, which makes the choice of the exchange-correlation functional particularly important.[6] The semilocal approximations to the exchange-correlation functionals often suffer from self-interaction error (SIE), which manifests itself in an incorrect asymptotic description of Coulomb interactions. The SIE can be mitigated by adding a portion of the Hartree−Fock (HF) exchange to semilocal density functionals. In the global hybrid functionals, the exchange-correlation potential decays as $-a/r$, where a is the fraction of HF exchange. To fix the long-range behavior, one can use range-separated or long-range-corrected (LRC) hybrid functionals. In these functionals, the Coulomb operator is split into short- and long-range parts, and the separation between the two is controlled by the range-separation parameter (traditionally called ω). The short-range Coulomb interaction is treated by standard functionals, whereas the long-range interaction is treated by the exact HF exchange. Our results illustrate the utility of different flavors of LRC hybrids in describing the emission spectra of exciplexes and underlying electronic properties.

METHODS

Choice of Functionals. From the rungs of the Jacob's ladder[40] of density functionals, we chose the commonly employed meta-GGAs and global and LRC hybrid functionals and assessed their performance in calculating the emission spectra and wave function properties. In this section, we justify their choice and highlight essential features that are relevant to this study.[7]

Meta-GGAs: M06-L,[41] revM06-L,[42] SCAN,[43] r^{2}SCAN,[44] and B97M-rV.[45] We selected recently developed meta-GGAs from various groups of developers. The Minnesota local functionals are characterized by a high degree of parametrization. These parameters are optimized through fitting to extensive energy databases. These databases include atomization energies, ionization potentials, electron affinities, barrier heights, noncovalent interactions, bond lengths, and frequencies. From the Minnesota family, we chose two meta-GGAs with the same functional form, M06-L[41] and revM06-L.[42] The exchange component combines a modified Voorhis−Scuseria XC (VSXC) type exchange[46] with another exchange term constructed by multiplying the Perdew−Burke−Ernzerhof (PBE)[47] enhancement factor with a parametrized kinetic energy density enhancement factor. The correlation energy combines both parallel-spin and opposite-spin components and follows a parametrized form developed by Becke[48] (Bc95), a form that gained popularity through VSXC.[46] The parameters for both the exchange and correlation in revM06-L were fitted to a considerably larger number of data sets compared to M06-L. As a result, revM06-L yields mean unsigned errors comparable to those of hybrid functionals when tested on various databases, including data sets for vertical excitation energies.[42]

In contrast to Minnesota functionals, the strongly constrained and appropriately normed (SCAN)[43] functional was constructed by imposing 17 known exact constraints. The SCAN functional shows numerical instability due to unphysical divergence of the exchange-correlation potential.[49] The rSCAN functional was introduced to mitigate this issue by modifying the iso-orbital indicator. Such modification lifted the constraint that forces the SCAN functional to follow exactly under a uniform scaling of density. Subsequently, the r^{2}SCAN functional was developed, which employs an improved form of the iso-orbital indicator. This results in a functional that not only satisfies all constraints but also is numerically stable and demonstrates better accuracy than rSCAN.[44] The performance of these functionals has been assessed by computing various solid-state properties.[50−52]

https://doi.org/10.1021/acs.jctc.4c00005
J. Chem. Theory Comput. 2024, 20, 2520−2537

A series of exchange-correlation functionals were constructed following the B97[53] functional developed by Becke. Though the B97 functional is a global hybrid functional, the isolated exchange and correlation parts have been used to construct a number of other meta-GGA and hybrid functionals. The B97M-rV[45] uses a meta-GGA version of B97 exchange and rVV10 nonlocal correction.[54] The B97M-rV functional yields small mean signed errors in interaction energies of noncovalent complex data sets[45] and errors comparable to M06-L for quasiparticle energies in vertical excitation databases.[17]

Global Hybrids: B3LYP,[55] B97,[53] PBE0,[56,57] B5050LYP,[58] SOGGA11-X,[59] TPSSh,[60] M06-2X,[61] and SCAN0.[62] The global hybrid (GH) functionals incorporate a fraction of the exact exchange, commonly referred to as the HF exchange. The general form for such hybrid functionals is

$$E_{XC}^{GH} = C_X E_X^{HF} + (1 - C_X)E_X^{DFA} + E_C^{DFA} \quad (1)$$

where C_X is the parameter determining the percentage of HF exchange. In some functionals, the value of C_X in the second term is zero, implying that 100% of a given exchange-correlation functional is used, alongside the C_X fraction of HF. The approximate treatment of the exchange E_X^{DFA} and correlation E_C^{DFA} can be a GGA or meta-GGA type. The HF contribution and underlying exchange-correlation functionals are given in Table S1 of the Supporting Information (SI). B3LYP,[55] B97,[53] PBE0,[56,57] B5050LYP,[58] SOGGA11-X[59] are GH GGA functionals, and TPSSh,[60] M06-2X,[61] and SCAN0[62] are GH meta-GGA functionals. The exact exchange-mixing parameter C_X is determined based on fitting to various experimental properties. For B3LYP, C_X is set by fitting to the heats of formation of small molecules.[55] In the case of B97, it is determined by fitting to atomization energies, ionization potentials, and proton affinities of the G2 data set.[63] For PBE0,[56] C_X is fixed to 0.25, the value derived from fourth-order perturbation theory.[64] The B5050LYP[58] and SOGGA11-X[59] functionals incorporate a relatively larger portion of HF exchange, 50 and 40.15%, respectively. The mixing parameter for B5050LYP was predefined. In the case of SOGGA11-X, the mixing parameter was determined by minimizing a training function consisting of a combination of different weighted root-mean-square errors (RMSEs) of thermochemistry data sets. For TPSSh, a very small fraction, $C_X = 0.10$, was determined by optimizing the mean absolute deviation in the enthalpies of formation for 223 molecules.[60] Along with C_X, all other parameters in the exchange-correlation functional form of M06-2X were derived by minimizing a training function based on the RMSEs or RMSE per bond across various energetic databases.[61] Similar to PBE0, the mixing parameter in SCAN0[62] is set at 0.25. The inclusion of a fraction of HF exchange into the functionals addresses the delocalization error, or SIE, inherent to semilocal functionals.[65−67]

Range-Separated Hybrids (GGA): CAM-B3LYP,[68] ωPBE,[69,70] ωB97X-D,[71] ωPBEh,[72] ωB97X-D3,[73] ωB97X-V,[74] M11,[75] ωM06-D3,[73] and ωB97M-V.[76] The exchange-correlation potentials of GGA, meta-GGA, and GH functionals decay incorrectly in the asymptotic region, which is why they cannot accurately describe CT complexes or predict properties such as excitation energies and polarizabilities in conjugated systems.[77,78] To overcome this problem, range-separated hybrid (RSH) functionals were developed, in which the Coulomb interaction $1/r$ is divided into short-range and long-range components by using an error function (erf),

$$\frac{1}{r} = \frac{1 - \mathrm{erf}(\omega r)}{r} + \frac{\mathrm{erf}(\omega r)}{r} \quad (2)$$

The first part of the right-hand side dominates at shorter separation and decays to zero on a length scale of approximately $\sim 1/\omega$. The second part corresponds to the long-range component, with the range separation being controlled by ω. Since the HF potential exhibits the correct asymptotic decay, 100% HF exchange is used in the long-range region. A standard representation for RSH functionals is as follows:

$$E_{XC}^{RSH} = C_X E_X^{SR-HF}(\omega) + (1 - C_X)E_X^{SR-DFA}(\omega) + E_X^{LR-HF}(\omega) + E_C^{DFA} \quad (3)$$

Here, C_X represents the short-range HF (SR-HF) mixing parameter. The term $(1 - C_X)$ corresponds to the short-range density functional exchange, and E_C^{DFA} is the density functional correlation energy applied across the entire range. In some functionals,[70,79,80] C_X is set to zero, which means that pure density functional is used in the short-range and pure HF treatment is used in the long-range. We chose RSH functionals with both GGA and meta-GGA approximations of SR-HF in this study. Of the GGA RSHs, ωPBE,[69,70] ωB97X-D,[71] ωPBEh,[72] ωB97X-D3,[73] and ωB97X-V[74] incorporate 100% HF in the long-range. Of the meta-GGA RSHs, ωM06-D3[73] and ωB97M-V[76] incorporate 100% HF in the long-range. Table S2 of the Supporting Information reports values of the range-separation parameter ω and the components of the considered RSH functionals. We selected CAM-B3LYP[68] as the representative of functionals based on the Coulomb attenuation method (CAM), in which the range-separation described in eq 2 is generalized with two parameters α and β as

$$\frac{1}{r} = \frac{1 - [\alpha + \beta \cdot \mathrm{erf}(\omega r)]}{r} + \frac{\alpha + \beta \cdot \mathrm{erf}(\omega r)}{r} \quad (4)$$

The parameter α denotes the HF contribution across the entire range, whereas the factor $1 - (\alpha + \beta)$ represents the fraction of the density functional over the same range. Several exchange-correlation functionals have been developed using the CAM method.[68,81,82]

A common procedure to optimize the parameters ω and C_X is the least-squares fitting of RMSEs of different ground-state properties, including atomization energies, barrier heights, and ionization energies. The development of ωPBE and ωPBEh functionals also included vertical excitation energies of organic molecules.[69,72] The functionals with B97 exchange were constructed with different flavors of dispersion corrections, and the corresponding HF mixing and range-separation parameters were optimized accordingly.[53] The ω values range from 0.2 to 0.33 across all GGA and meta-GGA type LRC functionals, with higher values indicating greater long-range HF contributions. A simple examination of the three B97-based RSH functionals reveals an inverse relationship between ω and C_X. This inverse relation is necessary for maintaining the balance in the proportion of exact exchange incorporated in the functionals. Except for the M11 functional, all other meta-GGA type RSHs have 100% HF in the long-range (Table S2 of Supporting Information). The M11 functional includes the same percentage, 57.2% of long-range HF and short-range density functional, along with 42.8% of HF in the short-range.[75]

Because semilocal functionals feature significant SIEs, they underestimate the energies of CT and Rydberg states. Therefore, the hybrid functionals are preferred for calculating

https://doi.org/10.1021/acs.jctc.4c00005
J. Chem. Theory Comput. 2024, 20, 2520−2537

the excitation energies of molecular complexes.[8,13,83,84] The fraction of the exact exchange included in a functional directly affects the vertical excitation energies and UV/vis absorption spectra.[85,86] An extensive study of excitation energies of a large test set has concluded that though Jacob's ladder of density functionals holds in TDDFT, the meta-GGA hybrids do not perform better than the GGA hybrids.[84] In this work, we extend the analysis to emission spectra of isolated [OPP-N]* (N = 3, 4) and their exciplexes, [OPP-3−TEA]* and [OPP-4−TEA]*, in various solvents.

Exciton Descriptors. Electronic transitions can be described as correlated electron−hole pairs or excitons.[19,27,28,34] The essential object for this description is the one-particle transition density matrix, γ^{FI}, connecting the ground Φ^{I} and excited Φ^{F} states:[19]

$$\gamma_{pq}^{\mathrm{FI}} = \langle \Phi^{\mathrm{F}} | \hat{\mathbf{p}}^{\dagger}\ \hat{\mathbf{q}} | \Phi^{\mathrm{I}} \rangle \tag{5}$$

where $\hat{\mathbf{p}}^{\dagger}$ and $\hat{\mathbf{q}}$ are the creation and annihilation operators corresponding to the ϕ_p and ϕ_q molecular orbitals, respectively. In TDDFT and configuration interaction singles (CISs), the elements of γ^{FI} are the amplitudes of the CIS states (when Φ^{I} is the ground-state determinant). In general, γ^{FI} provides a mapping between the two many-body states. When plotted in the coordinate space, it can be interpreted as the exciton wave function (χ_{exc})[87]

$$\chi_{\mathrm{exc}}(r_{\mathrm{h}}, r_{\mathrm{e}}) = \sum_{pq} \gamma_{pq}^{\mathrm{FI}} \phi_p(r_{\mathrm{h}}) \phi_q(r_{\mathrm{e}}) \tag{6}$$

where r_{h} and r_{e} denote the hole and electron (particle) coordinates. The squared norm of exciton wave function, Ω, quantifies single excitation character (e.g., it equals one for CIS and TDDFT transitions from the ground state).

Singular-value decomposition of γ^{FI} yields NTOs

$$\gamma^{\mathrm{FI}} = \mathbf{U}\Sigma\mathbf{V}^{T} \tag{7}$$

where Σ is a diagonal matrix of singular values and $\mathbf{U}$ and $\mathbf{V}$ are unitary transformations from the original molecular orbitals to a set of orbitals that compactly represent the hole and electron involved in the transition. The hole and electron NTOs, $\Psi_K^{\mathrm{e}}(r)$ and $\Psi_K^{\mathrm{e}}(r)$, are defined as

$$\Psi_K^{\mathrm{h}}(r) = \sum_q V_{qK} \phi_q(r) \tag{8}$$

and

$$\Psi_K^{\mathrm{e}}(r) = \sum_q U_{qK} \phi_q(r) \tag{9}$$

where K denotes the K^{th} NTO pair associated with singular value σ_K. NTOs provide the most compact representation of the electronic transitions.[88]

Using the exciton wave function, one can compute exciton descriptors as the expectation values of relevant operators. For instance, the position operator quantifies the average location of the hole or the electron. Using the exciton wave function, one can quantify the CT character by computing the vectorial distance between the centroids of electron and hole distributions, $d_{\mathrm{h}\to\mathrm{e}}$:

$$d_{\mathrm{h}\to\mathrm{e}} = \frac{1}{\Omega} |\langle \chi_{\mathrm{exc}} | r_{\mathrm{h}} - r_{\mathrm{e}} | \chi_{\mathrm{exc}} \rangle| \equiv |\langle (r_{\mathrm{h}} - r_{\mathrm{e}}) \rangle_{\mathrm{exc}}| \tag{10}$$

$d_{\mathrm{h}\to\mathrm{e}}$ quantifies permanent CT character, whereas a complementary descriptor, the exciton size, d_{exc}, describes dynamic CT (charge-resonance).

$$d_{\mathrm{exc}} = \sqrt{d_{\mathrm{h}\to\mathrm{e}}^2 + \sigma_{\mathrm{h}}^2 + \sigma_{\mathrm{e}}^2 - 2 \times \mathrm{COV}(r_{\mathrm{h}}, r_{\mathrm{e}})} \tag{11}$$

The exciton size takes into account the hole (σ_{h}) and electron (σ_{e}) sizes, as well as their covariance. The σ_{h} and σ_{e} quantify the root-mean-square deviation of the hole and electron distribution to their centroids and can be expressed mathematically as

$$\sigma_{\mathrm{h}} = \sqrt{\langle r_{\mathrm{h}}^2 \rangle_{\mathrm{exc}} - \langle r_{\mathrm{h}} \rangle_{\mathrm{exc}}^2} \tag{12}$$

and

$$\sigma_{\mathrm{e}} = \sqrt{\langle r_{\mathrm{e}}^2 \rangle_{\mathrm{exc}} - \langle r_{\mathrm{e}} \rangle_{\mathrm{exc}}^2} \tag{13}$$

The covariance normalized by the product of the electron and hole sizes gives the correlation coefficient (R_{eh}), a metric that describes the spatial correlation of the electron and hole motions

$$R_{\mathrm{eh}} = \frac{\mathrm{COV}(r_{\mathrm{h}}, r_{\mathrm{e}})}{\sigma_{\mathrm{h}}\sigma_{\mathrm{e}}} \tag{14}$$

Computational Procedure. All calculations were performed with Q-Chem[89] ab initio quantum chemistry software. Exciton properties were computed using the *libwfa* library.[27,34] Excited-state geometry optimizations and subsequent frequency calculations were carried out at the ωB97X-D3/aug-cc-pVDZ level of theory. Solvent effects were described with the conductor-like polarizable continuum model (C-PCM)[90,91] and the SMD[92] implicit solvation models. Five solvents were examined (dielectric constants: C_6H_{12} = 2.03, Bu_2O = 3.1, Et_2O = 4.34, PhBr = 5.2, and CH_2Cl_2 = 8.9). To describe the impact of out-of-equilibrium solvent effects on vertical $S_1 \to S_0$ emission, we used the state-specific approach.[93−96] We note that the out-of-equilibrium corrections are available for C-PCM but not yet available for SMD in Q-Chem.

*Isolated [OPP-N]**. The vertical emission energies of isolated OPP-N (N = 3, 4) were calculated as the energy difference between the first singlet excited state (S_1) and the corresponding ground-state energy, both computed at the excited-state minimum with the aug-cc-pVDZ basis. The exciton properties of the isolated chromophores were calculated with TDDFT/aug-cc-pVDZ and benchmarked against results from EOM-CCSD for excitation energies (EOM-EE-CCSD) with the 6-31+G* basis set. In EOM-EE-CCSD, the target states are described as single and double excitations from the reference CCSD wave function.[24] Hence, it describes multiconfigurational target states using single-reference formalism.[24,25] EOM-CC is capable of treating states of different character, such as local excitations and CT states on an equal footing.[24,25]

Exciplex. We used the ensemble of geometries constructed in our previous work as starting structures for exciplexes.[26] The [OPP-3−TEA]* ensemble comprises a total of 27 distinct geometries. These structures were reoptimized with TDDFT at the ωB97X-D3/aug-cc-pVDZ level of theory using cyclohexane (C_6H_{12}) as a solvent with the C-PCM solvation model. We employed the high-throughput workflow described in our previous work to refine our exciplex ensembles.[26] As we noted in our previous work,[26] the exciplex ensemble constructed using our procedure is not guaranteed to be complete but is nevertheless capable of reproducing experimental emission spectra accurately for the systems of interest. Of the initial 27 geometries, only 16 distinct structures remained after

https://doi.org/10.1021/acs.jctc.4c00005
J. Chem. Theory Comput. 2024, 20, 2520−2537

Table 1. $S_1 \rightarrow S_0$ Emission Energies (eV) of Isolated OPP-3 Calculated with TDDFT/aug-cc-pVDZ Using C-PCM; Oscillator Strengths Are Given in Parentheses

Functionals	Gas	CyHex	Bu_2O	Et_2O	PhBr	CH_2Cl_2
Experiment[23]		3.66	3.66	3.68	3.45	3.64
EOM-CCSD		3.95				
			Meta-GGAs			
M06-L	3.32 (1.12)	3.17 (1.34)	3.11 (1.45)	3.07 (1.50)	3.05 (1.52)	3.02 (1.57)
revM06-L	3.48 (1.19)	3.33 (1.44)	3.26 (1.53)	3.23 (1.58)	3.21 (1.61)	3.18 (1.66)
SCAN	3.46 (1.54)	3.27 (1.71)	3.19 (1.76)	3.15 (1.79)	3.13 (1.80)	3.09 (1.82)
r^2SCAN	3.33 (1.13)	3.19 (1.37)	3.13 (1.46)	3.09 (1.52)	3.08 (1.54)	3.04 (1.59)
B97M-rV	3.29 (1.10)	3.15 (1.34)	3.09 (1.43)	3.05 (1.48)	3.04 (1.50)	3.01 (1.55)
			Global Hybrids			
B3LYP	3.38 (1.12)	3.22 (1.33)	3.18 (1.45)	3.13 (1.47)	3.13 (1.51)	3.10 (1.56)
B97	3.37 (1.11)	3.18 (1.43)	3.18 (1.43)	3.14 (1.48)	3.13 (1.50)	3.01 (1.55)
PBE0	3.46 (1.17)	3.30 (1.37)	3.27 (1.49)	3.21 (1.51)	3.22 (1.55)	3.18 (1.60)
B5050LYP	3.60 (1.18)	3.43 (1.34)	3.41 (1.49)	3.34 (1.47)	3.37 (1.55)	3.34 (1.59)
SOGGA11-X	3.33 (1.14)	3.36 (1.47)	3.36 (1.47)	3.32 (1.52)	3.31 (1.54)	3.28 (1.59)
TPSSh	3.34 (1.12)	3.14 (1.44)	3.14 (1.44)	3.11 (1.49)	3.09 (1.51)	3.06 (1.56)
M06-2X	3.63 (1.14)	3.50 (1.37)	3.45 (1.46)	3.41 (1.51)	3.40 (1.53)	3.37 (1.58)
SCAN0	3.64 (1.53)	3.39 (1.75)	3.39 (1.75)	3.35 (1.78)	3.33 (1.79)	3.29 (1.81)
			Range-Separated Hybrids			
CAM-B3LYP	3.78 (1.48)	3.46 (1.34)	3.41 (1.42)	3.37 (1.47)	3.36 (1.49)	3.32 (1.54)
ωPBE	3.74 (1.12)	3.62 (1.36)	3.56 (1.44)	3.53 (1.49)	3.52 (1.51)	3.49 (1.56)
ωB97X-D	3.65 (1.12)	3.52 (1.35)	3.47 (1.44)	3.43 (1.49)	3.42 (1.53)	3.40 (1.57)
ωPBEh	3.68 (1.13)	3.54 (1.36)	3.51 (1.50)	3.45 (1.50)	3.47 (1.56)	3.43 (1.59)
ωB97X-D3	3.69 (1.12)	3.57 (1.35)	3.52 (1.43)	3.49 (1.48)	3.47 (1.50)	3.44 (1.55)
ωB97X-V	3.72 (1.10)	3.60 (1.33)	3.55 (1.41)	3.52 (1.46)	3.50 (1.48)	3.48 (1.53)
M11	3.77 (1.12)	3.66 (1.35)	3.60 (1.44)	3.57 (1.49)	3.56 (1.51)	3.53 (1.56)
ωM06-D3	3.79 (1.16)	3.67 (1.39)	3.62 (1.47)	3.58 (1.52)	3.57 (1.54)	3.54 (1.59)
ωB97M-V	3.66 (1.08)	3.55 (1.30)	3.50 (1.42)	3.47 (1.44)	3.59 (1.65)	3.56 (1.69)

Table 2. $S_1 \rightarrow S_0$ Emission Energies (eV) of Isolated OPP-4 Calculated with TDDFT/aug-cc-pVDZ Using C-PCM; Oscillator Strengths Are Given in Parentheses

Functionals	Gas	CyHex	Bu_2O	Et_2O	PhBr	CH_2Cl_2
Experiment[23]		3.39	3.39	3.40	3.32	3.27
EOM-CCSD		3.79				
			Meta-GGAs			
M06-L	3.00 (1.58)	2.88 (1.83)	2.88 (1.83)	2.79 (1.97)	2.78 (1.99)	2.75 (2.03)
revM06-L	3.16 (1.70)	3.02 (1.95)	3.02 (1.95)	2.94 (2.10)	2.92 (2.12)	2.89 (2.16)
SCAN	3.11 (2.13)	2.89 (2.12)	2.95 (2.26)	2.84 (2.30)	2.83 (2.31)	2.79 (2.32)
r^2SCAN	3.01 (1.60)	2.89 (1.85)	2.89 (1.85)	2.80 (1.99)	2.79 (2.01)	2.76 (2.06)
B97M-rV	2.99 (1.57)	2.86 (1.82)	2.86 (1.82)	2.78 (1.96)	2.76 (1.98)	2.74 (2.03)
			Global Hybrids			
B3LYP	3.11 (1.66)	2.98 (1.84)	2.93 (1.99)	2.89 (1.97)	2.89 (2.05)	2.86 (2.09)
B97	3.11 (1.61)	2.99 (1.85)	2.94 (1.94)	2.91 (1.98)	2.89 (2.00)	2.87 (2.05)
PBE0	3.19 (1.72)	3.07 (1.89)	3.02 (2.05)	2.98 (2.02)	3.02 (2.05)	2.95 (2.15)
B5050LYP	3.38 (1.76)	3.24 (1.88)	3.21 (2.05)	3.16 (2.01)	3.17 (2.10)	3.14 (2.13)
SOGGA11-X	3.32 (1.67)	3.21 (1.92)	3.16 (2.01)	3.13 (2.05)	3.11 (2.07)	3.09 (2.12)
TPSSh	3.06 (1.60)	2.93 (1.84)	2.88 (1.93)	2.85 (1.98)	2.84 (2.01)	2.81 (2.04)
M06-2X	3.42 (1.66)	3.31 (1.91)	3.26 (1.99)	3.23 (2.04)	3.22 (2.05)	3.19 (2.10)
SCAN0	3.36 (2.17)	3.20 (2.30)	3.14 (2.33)	3.10 (2.34)	3.09 (2.35)	3.06 (2.36)
			Range-Separated Hybrids			
CAM-B3LYP	3.39 (1.63)	3.28 (1.63)	3.23 (1.94)	3.20 (1.99)	3.19 (2.01)	3.17 (2.05)
ωPBE	3.57 (1.65)	3.46 (1.89)	3.41 (1.97)	3.38 (2.01)	3.37 (2.03)	3.35 (2.07)
ωB97X-D	3.47 (1.66)	3.36 (1.89)	3.33 (2.04)	3.28 (2.02)	3.28 (2.07)	3.26 (2.11)
ωPBEh	3.50 (1.75)	3.37 (1.90)	3.32 (1.98)	3.29 (2.03)	3.30 (2.12)	3.27 (2.12)
ωB97X-D3	3.52 (1.64)	3.41 (1.88)	3.37 (1.96)	3.34 (2.01)	3.33 (2.02)	3.30 (2.07)
ωB97X-V	3.55 (1.62)	3.45 (1.86)	3.40 (1.94)	3.37 (1.98)	3.36 (2.00)	3.34 (2.04)
M11	3.60 (1.63)	3.50 (1.88)	3.45 (1.97)	3.43 (2.02)	3.41 (2.04)	3.39 (2.08)
ωM06-D3	3.62 (1.69)	3.51 (1.92)	3.46 (2.01)	3.44 (2.05)	3.43 (2.07)	3.40 (2.11)
ωB97M-V	3.50 (1.60)	3.40 (1.82)	3.45 (1.97)	3.42 (2.01)	3.44 (2.19)	3.30 (2.03)

https://doi.org/10.1021/acs.jctc.4c00005
J. Chem. Theory Comput. 2024, 20, 2520−2537

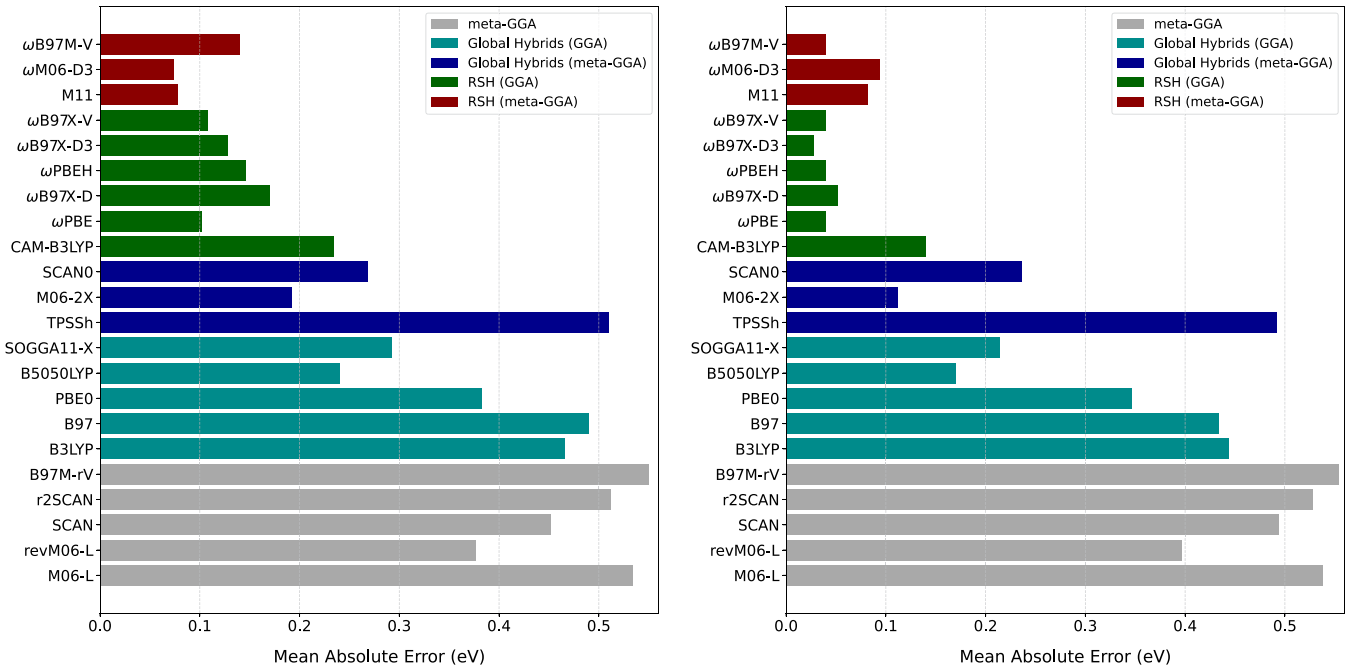

(a) OPP-3* (b) OPP-4*

Figure 1. MAE (eV) for all considered functionals with the C-PCM solvation model, determined by comparing the calculated emission energies of isolated chromophores ([OPP-3]* and [OPP-4]*) in all solvents to their corresponding experimental values.

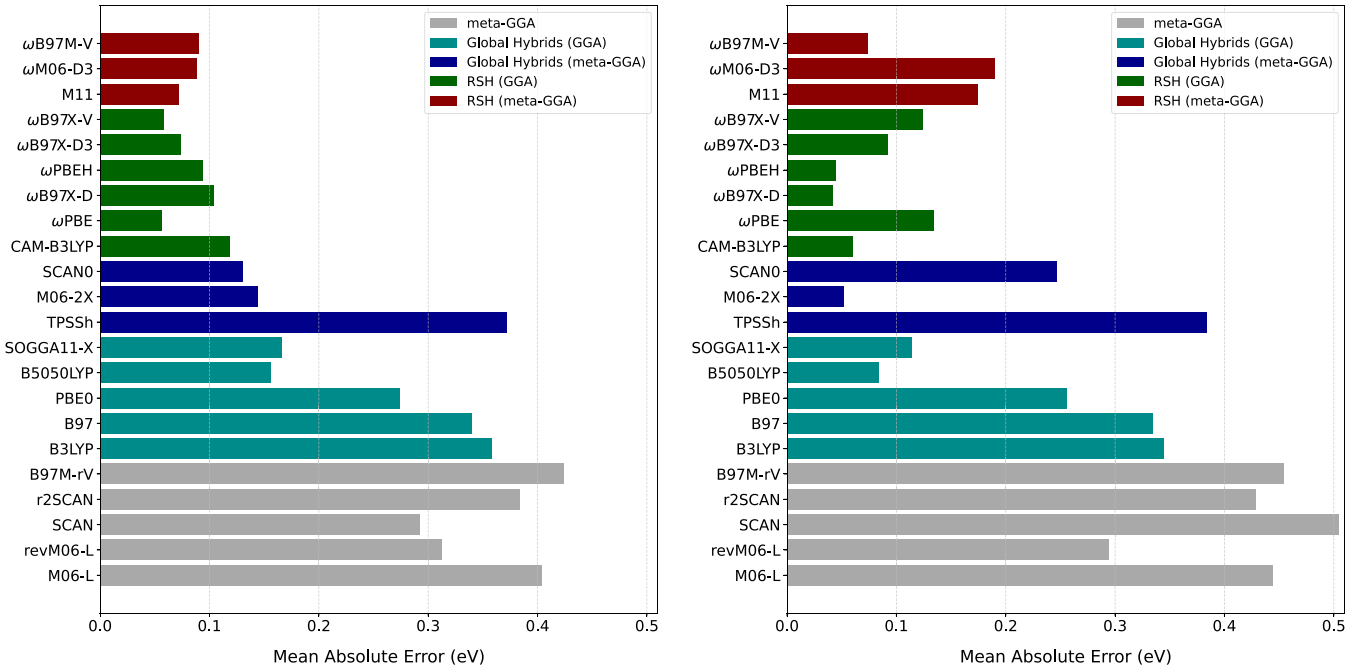

(a) OPP-3* (b) OPP-4*

Figure 2. MAE (eV) for all considered functionals with the SMD solvation model, determined by comparing calculated emission energies of isolated chromophores ([OPP-3]* and [OPP-4]*) in all solvents to their corresponding experimental values.

eliminating duplicate geometries. Subsequently, we verified that these 16 complexes indeed represent exciplexes by (1) computing vibrational frequencies to verify minima and (2) using excited-state energy decomposition analysis[97,98] to confirm that CT interactions are significantly larger than frozen or polarization terms. Following the same workflow as that for [OPP-4−TEA]* exciplexes, 15 unique structures emerged from the initial set of 25 geometries. Five of the remaining 10 structures converged to geometries already present in the set, and the remaining 5 did not exhibit significant CT from TEA to OPP-4*.

https://doi.org/10.1021/acs.jctc.4c00005
J. Chem. Theory Comput. 2024, 20, 2520−2537

The emission spectra for exciplexes were constructed by using oscillation strengths (f) and excitation energies (ε_i) computed for the ensemble, with a Boltzmann weight assigned to every structure,

$$p_i = \frac{e^{-(\varepsilon_i - \bar{\varepsilon})/(kT)}}{\sum_j e^{-(\varepsilon_j - \bar{\varepsilon})/(kT)}} \quad (15)$$

Here, $\bar{\varepsilon}$ is the mean of energy of all exciplex structures, k is the Boltzmann constant, and $T = 298$ K. The computed spectra were convoluted with Gaussians (full width at half-maximum = $2\sqrt{2\ln(2)}\,\sigma \approx 2.35482\sigma$, σ = 0.4 eV). The resulting spectra were converted to the wavelength (nm) scale[26] and benchmarked against experimental spectra.[23]

We also investigated the effect of density functionals on solvatochromic shifts. Solvent effects were examined for exciplex ensembles identified with cyclohexane (CyHex) without carrying out reoptimization of the geometries of the chromophore-donor complexes in diethyl ether (Et_2O). As our previous study showed that the SMD model yields solvatochromic shifts that are closer to the experiment compared to C-PCM, we employed SMD to probe functional accuracies in predicting solvatochromism.[26]

RESULTS AND DISCUSSION

Emission Energies of Isolated Chromophores. Tables 1 and 2 compare the experimental and calculated emission energies of [OPP-3]* and [OPP-4]*, respectively, in the gas phase and in the solution described by the C-PCM model. The mean absolute errors (MAEs) calculated across all solvents are shown in Figures 1 and 2 for the C-PCM and SMD models, respectively.

Meta-GGAs drastically underestimate the emission energies of [OPP-3]* and [OPP-4]* relative to the experiment. Of the meta-GGAs, B97M-rV and M06-L yield the highest MAEs in emission energies, while revM06-L yields the lowest. The MAE for r^{2}SCAN is slightly higher (0.06 eV) than SCAN. Owing to the partial SIE correction through HF exchange, the global hybrid meta-GGAs, SCAN0 and M06-2X, yield emission energies that are closer to the experiment than their meta-GGA counterparts. Of the global hybrid meta-GGAs, the one with the lowest fraction of HF exchange, TPSSh, unsurprisingly yields emission energies that deviate the most from experiment. The global hybrid GGAs yield emission energies that are slightly closer to the experiment than meta-GGAs. B5050LYP, which includes a larger fraction of the HF exchange relative to B3LYP, shows a significant improvement in emission energies. Across GGA and meta-GGA global hybrids, M06-2X is the best-performing functional.

The RSH functionals yield the lowest errors in emission energies. With the exception of CAM-B3LYP, MAEs of emission energies are lower than 0.2 eV for both RSH GGAs and RSH meta-GGAs. CAM-B3LYP, which combines the hybrid properties of B3LYP with LRC treatment, yields significantly improved energies over B3LYP but performs only slightly better than B5050LYP. Although the MAEs are similar across GGAs and meta-GGAs, all RSH meta-GGAs overestimate the emission energies of [OPP-4]*. The M11 functional, for instance, yields an accurate emission energy for [OPP-3]*, likely due to error cancellation as it overestimates the emission energies of [OPP-4]*. LRC functionals, ωPBEh and ωPBE, show comparable accuracies even though the latter does not include short-range HF exchange. Emission energies computed with ωPBE are slightly higher than those computed with ωPBEh by 0.05 to 0.08 eV. The MAE exhibited by ωPBE is smaller than ωPBEh by 0.04 and 0.02 eV for [OPP-3]* and OPP-4]*, respectively.

Solvent effects calculated with the SMD model for [OPP-3]* and [OPP-4]* emissions are shown in Tables S3 and S4 of the Supporting Information, respectively. The SMD model results in improved emission energies for meta-GGA relative to C-PCM, with MAEs shown in Figure 2. However, unlike C-PCM, SMD fails to capture the small solvatochromic shift (0.12 eV, CyHex → CH_2Cl_2) observed experimentally for [OPP-4]*. Use of the SMD model results in nearly identical emission energies and oscillator strengths for all of the solvents. As is to be expected of implicit solvation models, both C-PCM and SMD fail to capture the π-stacking interaction of [OPP-3]* with the aromatic bromobenzene (PhBr) solvent, which we believe significantly lowers the emission energy of [OPP-3]* in PhBr. The lowering is more pronounced in [OPP-3]* because, unlike in [OPP-4]*, it possesses a flat, planar geometry that is amenable to more favorable interactions with an arene solvent.

C-PCM solvation yields slightly red-shifted emission energies and brighter transitions with increasing solvent dielectric constant. The excited-state wave function becomes ionic and stabilized by a more polar solvent, leading to red-shifted energies. However, the range of experimental solvatochromic shifts is small (excluding PhBr, the range is 0.04 eV for [OPP-3]* and 0.13 eV for [OPP-4]*). Resolution of this narrow range will likely require explicit solvation models or higher levels of theory. Nevertheless, the small solvatochromic shifts observed for these isolated chromophores are captured by TDDFT and C-PCM across all of the functionals examined in this study.

We carried out a preliminary analysis of whether reoptimization of the geometries at the desired level of theory results in significant changes in emission energies. Table S5 in the Supporting Information shows emission energies of [OPP-3]* in different solvents (with both SMD and C-PCM models) with the excited-state geometry reoptimized at the ωPBE/aug-cc-pVDZ level of theory. The energies are blue-shifted by a very small amount (≈0.03 eV) relative to the reported emission energies for ωPBE/aug-cc-pVDZ in Table 1. The two solvation models also exhibit similar trends. The MAEs of emission energies in Table S5 are about 0.04 eV lower than those reported in Figures 1 and 2.

Exciton Analysis in Isolated Chromophores. We further examined the character of the $S_1 \rightarrow S_0$ transition in OPP-3 by using NTOs and exciton descriptors. Unlike the canonical KS orbitals, NTOs and the respective exciton descriptors provide rigorous and quantitative description of the excited-state character,[99] facilitating the comparisons between different levels of theory.[19] The exciton size and correlation coefficient (R_{eh}) are important descriptors of electronic structure in π-conjugated molecules—the former allows characterization of the exciton and the latter describes the electron−hole correlation.

Figure 3 shows the NTOs for the $S_1 \rightarrow S_0$ transition in OPP-3 computed with ωPBE/aug-cc-pVDZ. We chose this functional because it most closely reproduces the experimental emission energies for the isolated chromophores (MAE of 0.10 eV for [OPP-3]* and 0.04 eV for [OPP-4]*). As expected, this transition corresponds to a $\pi \rightarrow \pi^*$ excitation, and the transition character does not change upon solvation. All functionals examined in this study yield the same transition character. Figure S1 of the Supporting Information shows a similar $\pi \rightarrow \pi^*$ character for [OPP-4]*, except that the exciton is more localized

https://doi.org/10.1021/acs.jctc.4c00005
J. Chem. Theory Comput. 2024, 20, 2520−2537

Table 3. Exciton Descriptors for the $S_1 \rightarrow S_0$ Transition inOPP-3[a]

Functionals	Hole size (Å)	Electron Size (Å)	Exciton Size (Å)	Correlation Coefficient
EOM-CCSD	3.474	3.602	4.452	0.209
		Meta-GGAs		
M06-L	3.810	3.852	5.633	−0.081
revM06-L	3.786	3.815	5.514	−0.052
SCAN	3.849	3.874	5.494	−0.012
r^{2}SCAN	3.820	3.851	5.653	−0.086
B97M-rV	3.813	3.864	5.608	−0.067
		Global Hybrids		
B3LYP	3.724	3.802	5.303	0.007
B97	3.699	3.775	5.267	0.007
PBE0	3.673	3.752	5.171	0.030
B5050LYP	3.557	3.662	4.705	0.151
SOGGA11-X	3.601	3.702	4.890	0.103
TPSSh	3.752	3.815	5.452	−0.038
M06-2X	3.550	3.657	4.768	0.125
SCAN0	3.687	3.760	4.980	0.106
		Range-Separated Hybrids		
CAM-B3LYP	3.517	3.621	4.620	0.162
ωPBE	3.429	3.529	4.345	0.220
ωB97X-D	3.474	3.570	4.471	0.195
ωPBEh	3.473	3.571	4.489	0.188
ωB97X-D3	3.446	3.544	4.358	0.223
ωB97X-V	3.431	3.534	4.292	0.241
M11	3.438	3.566	4.367	0.223
ωM06-D3	3.434	3.521	4.327	0.226
ωB97M-V	3.441	3.559	4.344	0.231

[a]Oscillator strengths are given in parentheses. Hole size (σ_h), electron size (σ_e), and exciton size (d_{exc}) are given in Å. The correlation coefficient (R_{eh}) is dimensionless.

on the inner phenyl rings. This is consistent with the small increase in exciton size (Tables 3 and S6, Supporting Information) on going from [OPP-3]* to [OPP-4]*.

Table 3 reports the computed hole size, electron size, exciton size, and correlation coefficient for the $S_1 \rightarrow S_0$ transition in OPP-3. We assess the quality of exciton wave functions computed with various functionals by comparing the exciton descriptors against higher-level ab initio results from EOM-CCSD. Table 3 shows similar hole and electron sizes for the considered functionals, which is consistent with the local excitation character in the isolated [OPP-*N*]*. In comparison with EOM-CCSD, the meta-GGA functionals yield the largest hole and electron sizes. RSH functionals yield the best agreement with EOM-CCSD. Meta-GGA and global hybrid functionals yield more delocalized excitons (relatively larger exciton size). This is a consequence of the poor description of the electron−hole Coulomb interaction arising from intrinsic SIE. SIE is reduced in RSH functionals, resulting in improved values of exciton sizes.

Table 3 shows the large spread in values of the correlation coefficient computed with various functionals for [OPP-3]*. The correlation coefficient provides a measure of the spatial correlation between the hole and the electron motions. A positive electron−hole correlation coefficient (R_{eh}) defines a bound exciton because the electron position changes in the same direction as the hole position. Anticorrelated electron and hole pairs feature a negative R_{eh} value, and an R_{eh} value of zero indicates independent electron and hole quasi-particles.[19] All meta-GGA functionals as well as the TPSSh functional yield an anticorrelated electron−hole in contrast to EOM-CCSD. Again, the poor description of the R_{eh} values by these functionals results from their intrinsic SIE. The global hybrids yield a bound exciton, although the magnitude of R_{eh} is about 100 times smaller compared to EOM-CCSD. As expected, RSHs agree better with the EOM-CCSD results. Table S6 of the Supporting Information shows a similar trend in the exciton properties of [OPP-4]*. The ability of the functionals to accurately compute emission energies of the isolated molecules is, therefore, also manifested in the exciton properties, with meta-GGAs and TPSSh yielding anticorrelated electron−hole pairs and underestimating emission energies and RSH functionals accurately describing both the exciton properties and emission energies.

Emission Spectra of Exciplexes. We used the ensemble of 16 [OPP-3−TEA]* structures to calculate the emission spectra and peak maximum. Table 4 presents the peak positions (in nanometers and eV) for all the functionals. The table also shows the experimental peaks[23] for two solvents, CyHex and Et_2O, along with the solvatochromic shifts.

Note that the format for presenting exciplex data in these tables differs from that used for isolated chromophore data. In the exciplex tables, we specifically present the signed differences (SDs) from the experimental observations in each case. Figure 4 shows the experimental and computed spectra in CyHex. Figure S2 in the Supporting Information shows the spectra in Et_2O. For CyHex, the experimental peak is at 428 nm (2.89 eV), and for Et_2O, it is at 460 nm (2.69 eV). Going from CyHex to Et_2O, a redshift in the emission peak at 32 nm is observed.

In both solvents, all considered meta-GGA functionals yield very low emission energies and significantly red-shifted emission peaks relative to those of the experiment. The revised version of M06-L, revM06-L, yields improved estimates of emission peaks compared to M06-L. In CyHex and Et_2O solvents, revM06-L shows improvements in estimating emission peaks by 140 and 176 nm, respectively, when compared to the original M06-L. The emission peaks of r^{2}SCAN are more red-shifted relative to the SCAN values. The three meta-GGAs—M06-L, revM06-L, and B97M-rV—yield slightly higher energies compared to those of SCAN and r^{2}SCAN. This increase may be attributed to the fact that the underlying parameters of these three functionals are determined from thermochemistry data sets and are specifically constructed for molecular complexes. These large errors by meta-GGA functionals are expected for intermolecular CT

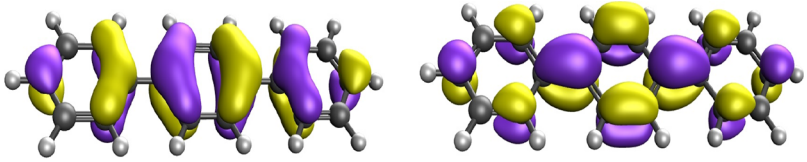

Figure 3. Hole (left) and electron NTOs (right) of [OPP-3]* in cyclohexane at the ωPBE/aug-cc-pVDZ level of theory with the C-PCM solvation model (isovalue = 0.2).

https://doi.org/10.1021/acs.jctc.4c00005
J. Chem. Theory Comput. 2024, 20, 2520−2537

Table 4. Peak Maxima (in Nanometers, with Values in eV in Parentheses) of the Emission Spectra of [OPP-3−TEA]*[a]

Functionals	CyHex nm (eV)	SD nm (eV)	Et_2O nm (eV)	SD nm (eV)	Shift nm	SD nm
Experiment[23]	428 (2.89)		460 (2.69)		32	
			Meta-GGAs			
M06-L	950 (1.30)	522 (−1.59)	1090 (1.14)	630 (−1.55)	140	108
revM06-L	810 (1.53)	382 (−1.36)	914 (1.35)	454 (−1.34)	104	072
SCAN	986 (1.26)	558 (−1.63)	1132 (1.09)	672 (−1.60)	146	114
r^2SCAN	1034 (1.20)	606 (−1.69)	1203 (1.03)	743 (−1.66)	169	137
B97M-rV	859 (1.44)	431 (−1.45)	967 (1.28)	507 (−1.41)	108	076
			Global Hybrids			
B3LYP	676 (1.83)	248 (−1.06)	735 (1.69)	275 (−1.00)	59	27
B97	695 (1.78)	267 (−1.11)	760 (1.63)	300 (−1.06)	65	33
PBE0	651 (1.90)	223 (−0.99)	702 (1.77)	242 (−0.92)	51	19
B50S0LYP	422 (2.94)	−6 (0.05)	434 (2.86)	−26 (0.17)	12	−20
SOGGA11-X	487 (2.54)	059 (−0.35)	510 (2.43)	050 (−0.26)	23	−09
TPSSh	815 (1.52)	387 (−1.37)	909 (1.36)	449 (−1.33)	94	62
M06-2X	456 (2.72)	028 (−0.17)	475 (2.61)	015 (−0.08)	19	−13
SCAN0	582 (2.13)	154 (−0.76)	622 (1.99)	162 (−0.70)	40	08
			Range-Separated Hybrids			
CAM-B3LYP	458 (2.71)	30 (−0.18)	476 (2.60)	16 (−0.09)	18	−14
ωPBE	440 (2.82)	12 (−0.07)	456 (2.72)	−4 (0.03)	16	−16
ωB97X−D	455 (2.72)	27 (−0.17)	474 (2.62)	14 (−0.07)	19	−13
ωPBEh	475 (2.61)	47 (−0.28)	497 (2.49)	37 (−0.20)	22	−10
ωB97X−D3	419 (2.96)	−9 (0.07)	432 (2.87)	−28 (0.18)	13	−19
ωB97X−V	393 (3.15)	−35 (0.26)	402 (3.08)	−58 (0.39)	09	−23
M11	404 (3.07)	−24 (0.18)	415 (2.99)	−45 (0.30)	11	−21
ωM06-D3	387 (3.20)	−41 (0.31)	395 (3.14)	−65 (0.45)	08	−24
ωB97M-V	403 (3.07)	−25 (0.18)	412 (3.01)	−48 (0.32)	09	−23

[a]The SD values from the experimental peak are also shown. The last two columns report the observed solvatochromic shift in nm and the deviation from the experimental shift.

molecules as these functionals have SIE, and their exchange-correlation potentials are incorrect for long-range Coulomb interactions.

The accuracy of global hybrid functionals for excitation energies depends more on the percentage of exact exchange included in the functionals than on whether they are classified as GGA or meta-GGA type global hybrids.[84,100,101] Among GGA-type global hybrids, B50S0LYP (50% HF exchange) and SOGGA11-X (40.15% HF exchange) are very close to the experimental emission peaks (SD of −6 and 59 nm, respectively). In the case of meta-GGA type global hybrids, TPSSh, with only 10% HF, results in the largest SD from experiment, making it the worst performing hybrid functional chosen in this study. The observed trends for global hybrids are similar for both solvents (Table 4). M06-2X's solvatochromic shift of 19 nm stands out as the most accurate among functionals whose peak positions fall within 30 nm of the experimental data. These findings confirm that global hybrid functionals with a substantial percentage of exact exchange can be suitable for excited-state studies of intermolecular CT complexes.

All RSH functionals chosen in this study exhibit deviations under 50 nm in CyHex and 65 nm in Et_2O from the experimental peaks. The accuracy is governed by the inverse relationship between two parameters, ω and C_X, which control the exact exchange used in short and long ranges to minimize both localization and delocalization errors. The balance between these parameters is crucial for accurately describing fractional CT and excitation properties.[102] Figure 4d,e shows the emission spectra computed with RSH-GGA and RSH-meta-GGA functionals, respectively. Among the RSH-GGA, ωPBEh is the most red-shifted, whereas ωB97X-V is the most blue-shifted relative to the experiment. ωPBE and ωB97X-D3 are closest to the experiment, with peak positions deviating by only 12 and −9 nm, respectively. All of the RSH-meta-GGA functionals show comparatively large emission energies, resulting in significantly blue-shifted spectra [Figure 4e] compared to both the experiment and most of the RSH GGAs. With the peak positioned at 387 nm, the ωM06-D3 functional is the most blue-shifted (41 nm from experiment). In Et_2O solvent (Figure S2 of the Supporting Information), ωPBE and ωB97X-D spectra are the closest to the experiment. Similar to observations in CyHex, RSH meta-GGAs in Et_2O overestimate emission energies, resulting in blue-shifted spectra. The solvatochromic shifts observed with these functionals are significantly smaller compared with the experimental data.

To provide an overall view of the functional accuracy in computing emission spectra, Figure 5 shows the mean signed error (ME) and mean absolute error (MAE) in nanometers, considering the functional performance in both CyHex and Et_2O. ωPBE emerges as the most accurate functional for excited-state intermolecular CT systems. Additionally, the B50S0LYP and M06-2X global hybrid functionals exhibit superior accuracy compared with most of the range-separated functionals. RSH meta-GGAs do not offer significant improvements over RSH-GGA.

Table 5 reports the emission peak maxima for [OPP-4−TEA]* exciplexes computed with 12 hybrid functionals. This table excludes other functionals with emission peak errors exceeding 100 nm in the case of [OPP-3−TEA]*. Figures S3 and S4 in the Supporting Information compare the emission spectra computed by these functionals in CyHex and Et_2O with the experiment. Figure 6 shows the mean errors and MAEs for

https://doi.org/10.1021/acs.jctc.4c00005
J. Chem. Theory Comput. 2024, 20, 2520−2537

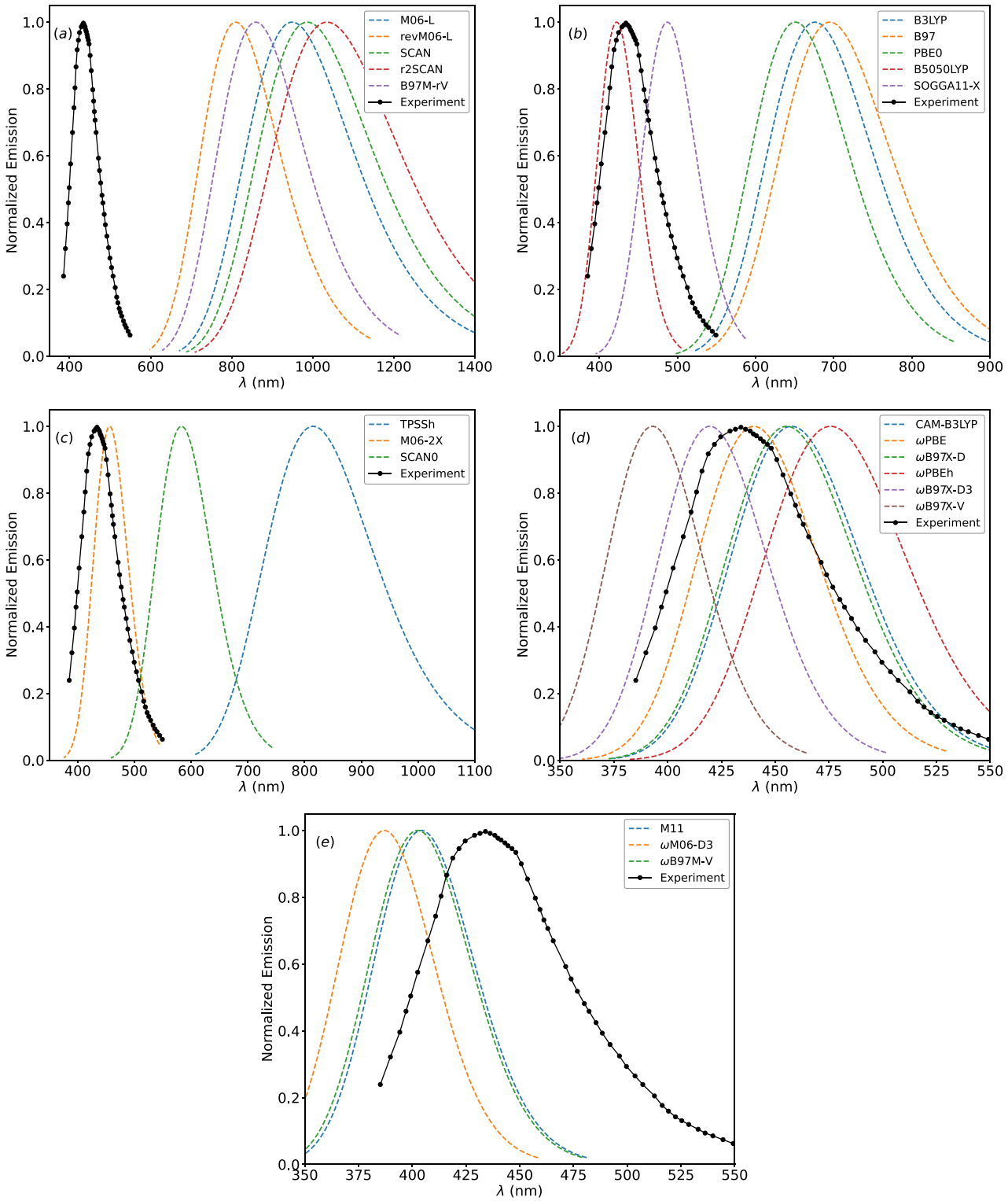

Figure 4. Emission spectra of [OPP-3−TEA]* computed with different density functionals along with the experimental spectra in CyHex solvent. (a) Meta-GGA functionals, (b) global hybrid (GGA), (c) global hybrid (meta-GGA), (d) RSH (GGA), and (e) RSH (meta-GGA).

the data reported in Table 5. Three RSH meta-GGAs, i.e., M11, ωM06-D3, and ωB97M-V, overestimate the emission energies in both solvents, resulting in significantly blue-shifted spectra. In CyHex, the ωPBE peak aligns almost perfectly with the experimental spectrum, with the M06-2X and ωB97X-D peaks deviating by 14 and 16 nm, respectively. The ωB97X-V functional exhibits the most blue-shifted spectrum among all considered RSH GGAs. In the Et_2O solvent, ωB97X-V continues to yield the most blue-shifted spectrum, with a peak at 399 nm, a substantial 71 nm deviation from the experimental value. The emission peak positions for M06-2X, CAM-B3LYP, and ωB97X-D are closest to the experimental peak at 470 nm. As Table S6 shows, the four functionals—M06-2X, ωB97X-D, ωPBE, and CAM-B3LYP—are within 10 nm of experimental

https://doi.org/10.1021/acs.jctc.4c00005
J. Chem. Theory Comput. 2024, 20, 2520−2537

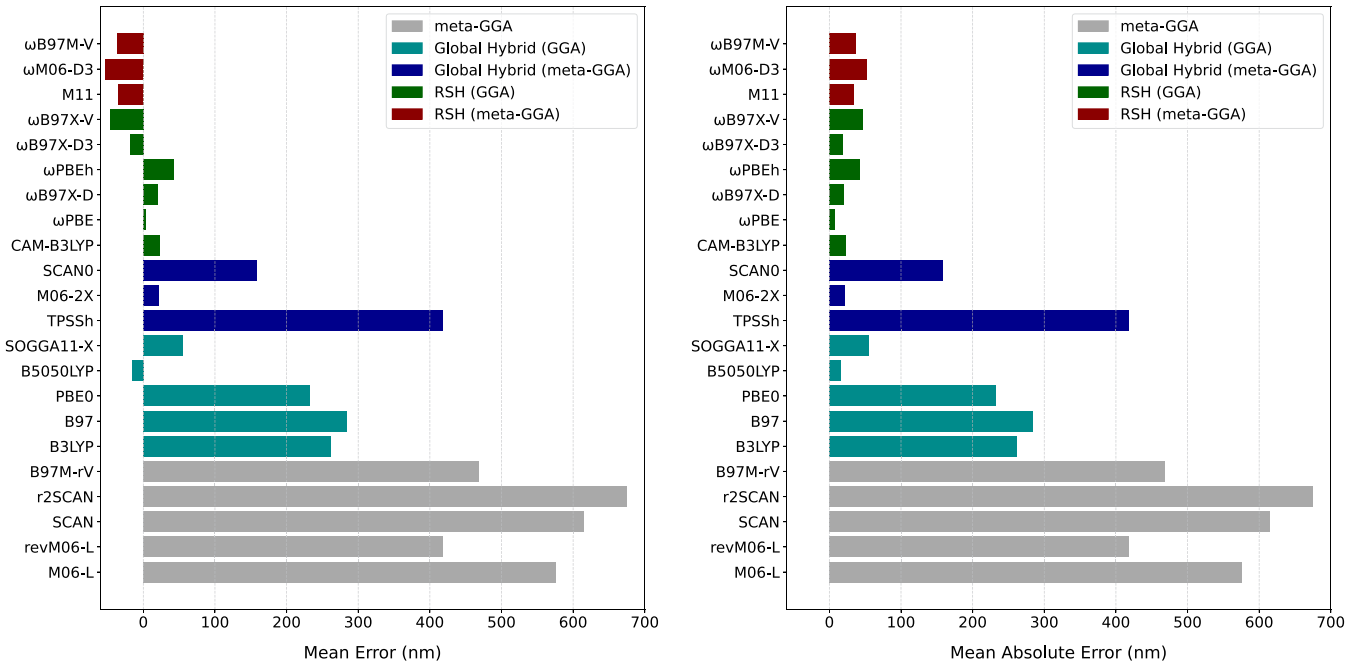

Figure 5. Left panel shows mean error (in nm) for all considered functionals, as determined by comparing [OPP-3-TEA]* exciplex emission peaks in both CyHex and Et_2O solvents to experimental values. The right panel shows absolute errors.

Table 5. Peak Maxima (in nm, with Values in eV in Parentheses) of the Emission Spectra of [OPP-4−TEA]*[a]

Functionals	CyHex nm (eV)	SD nm (eV)	Et_2O nm (eV)	SD nm (eV)	Shift nm	SD nm
Experiment[23]	444 (2.79)		470 (2.64)		26	
B5050LYP	420 (2.95)	−24 (0.16)	430 (2.88)	−40 (0.24)	10	−16
SOGGA11-X	492 (2.52)	48 (−0.27)	506 (2.45)	36 (−0.19)	14	−12
M06-2X	458 (2.71)	14 (−0.08)	469 (2.64)	−01 (0.00)	11	−15
CAM-B3LYP	462 (2.68)	18 (−0.17)	471 (2.63)	01 (−0.01)	09	−17
ωPBE	448 (2.77)	04 (−0.02)	457 (2.71)	−13 (0.07)	09	−17
ωB97X-D	460 (2.69)	16 (−0.10)	469 (2.64)	−01 (0.00)	09	−17
ωPBEh	487 (2.54)	43 (−0.25)	505 (2.45)	35 (−0.19)	18	−08
ωB97X-D3	418 (2.96)	−26 (0.17)	426 (2.91)	−44 (0.27)	08	−18
ωB97X-V	391 (3.17)	−53 (0.38)	399 (3.11)	−71 (0.47)	08	−18
M11	403 (3.07)	−41 (0.28)	407 (3.05)	−63 (0.41)	04	−22
ωM06-D3	387 (3.20)	−57 (0.41)	394 (3.15)	−76 (0.51)	07	−19
ωB97M-V	401 (3.09)	−43 (0.30)	409 (3.03)	−61 (0.39)	08	−18

[a]The SD values from the experimental peak are also shown. The last two columns report the observed solvatochromic shift in nm and the deviation from the experimental shift.

emission peaks, on average. The high accuracy of B5050LYP and ωB97X−D3 observed in [OPP-3−TEA]* is not reproduced in [OPP-4−TEA]* exciplexes, for which these functionals yield emission peaks that are blue-shifted by over 20 nm in CyHex and more than 40 nm in Et_2O. All functionals examined underestimate the solvatochromic shift from CyHex to Et_2O observed for the [OPP-4−TEA]* exciplex. The best-performing functionals yield solvatochromic shifts smaller than 12 nm, significantly lower than the experimentally observed value of 26 nm. This underestimation is particularly pronounced for the RSH meta-GGAs.

Another spectroscopic observable against which we benchmark is the shift of the emission peak between OPP-3 and OPP-4 exciplex spectra. Experimentally, this shift is 16 nm in CyHex and 10 nm in Et_2O. Similar to our previous study, we assume that the σ values are identical for the two systems in order to construct the broadened spectra.[26] Upon comparing the emission peak maxima for the functionals listed in Table 5 with the corresponding values in Table 4, it becomes clear that the ωPBEh functional yields the closest shift to experimental values in both solvents, with a 12 nm shift in CyHex and an 8 nm shift in Et_2O. Following closely is the ωPBE functional, showing an 8 nm shift in CyHex and a 1 nm shift in Et_2O. One possible reason for their better performance is the fact that both ωPBE and ωPBEh functionals included the vertical excitation energy test set in their parametrization. Whereas a positive shift from [OPP-3-TEA]* to [OPP-4-TEA]* is observed with the SOGGA11-X, M06-2X, CAM-B3LYP, and ωB97X-D functionals in CyHex, most functionals fail to predict a positive shift in Et_2O.

Tables S7 and S8 summarize functional performances by class for CyHex and Et_2O solvents, respectively, and report the functional(s) within each class that yield the smallest error in emission energy for isolated excited state and exciplex emissions for OPP-3 and OPP-4. Analyzing functionals across different rungs reveals that RSH GGAs maintain a satisfactory level of

https://doi.org/10.1021/acs.jctc.4c00005
J. Chem. Theory Comput. 2024, 20, 2520−2537

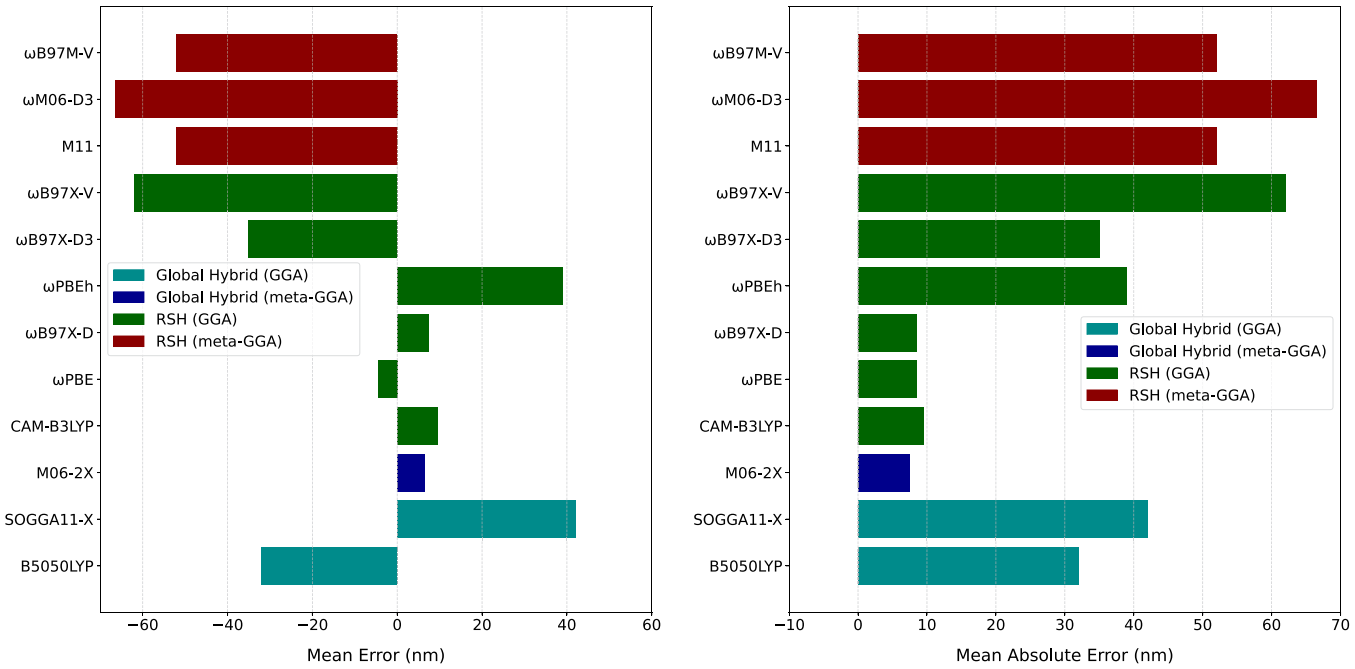

Figure 6. Error bar plots for various functionals for the emission peak maxima of [OPP-4−TEA]* exciplexes. The left panel shows the mean error in nanometers for all considered functionals, as determined by comparing emission peaks in both CyHex and Et_2O solvents to experimental values. The right panel shows the absolute errors.

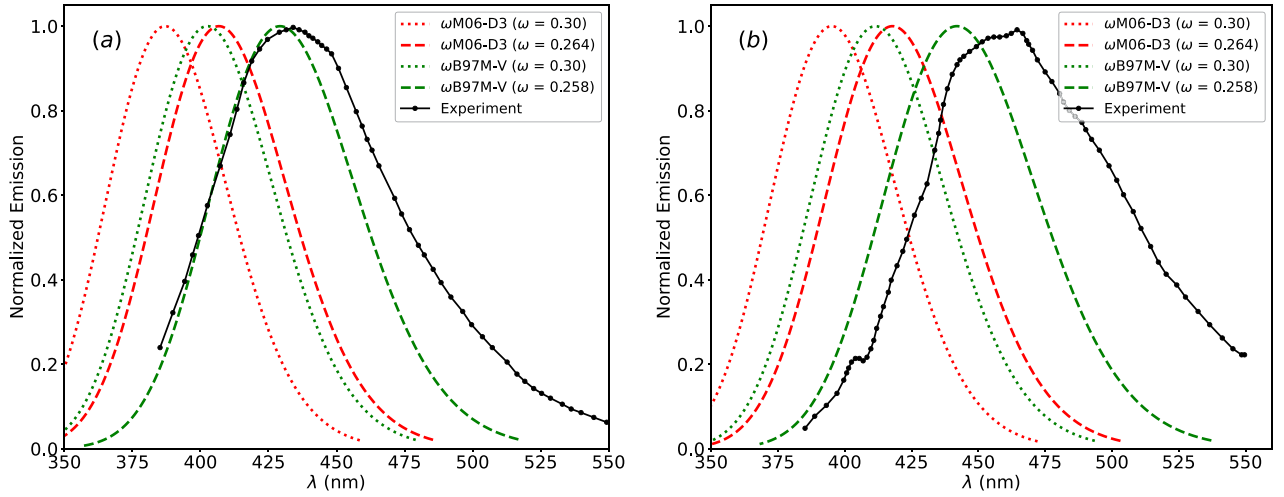

Figure 7. Emission spectra computed with ωM06-D3 and ωB97M-V with the original and tuned ω values. The experimental normalized emissions for two solvents, (a) CyHex and (b) Et_2O, are shown in black. The ωM06-D3 and ωB97M−V results are shown in red and green, respectively.

accuracy. Specifically, ωPBE emerges as a suitable choice for intermolecular CT excitations. The improved accuracy of ωPBE can be attributed to the inclusion of excitation data sets during the training phase for the exact exchange parameter determination. In addition, the substantial percentage of HF exchange in global hybrids, specifically in B5050LYP and M06-2X, allows them to describe excitations with reasonable accuracy. However, the RSH meta-GGAs consistently yield larger emission energies, resulting in blue-shifted spectra relative to experiment. Owing to their relatively higher ω, functionals such as ωM06-D3 and ωB97M-V yield the largest blue shifts. These shifts are the likely result of overlocalization caused by the inclusion of both short-range HF and 100% long-range HF in these functionals.[102]

It is possible to fine-tune ω for the system of interest.[103] The tuning entails varying ω to satisfy the exact condition so that the Koopmans ionization energy (IE) (energy of KS HOMO) becomes equal to the difference in the total KS energies (ΔSCF) of the neutral and ionized systems:

$$\epsilon_{\mathrm{HOMO}}(\omega) = -\Delta\mathrm{SCF} = -\mathrm{IE}(\omega) \tag{16}$$

The ω dependence of both left- and right-hand sides of eq 16 needs multiple self-consistent calculations for both the neutral and ionized complex, with varying values of ω. However, due to the problematic system-size dependence[104,105] of ω derived from eq 16, an alternative method, known as the global density-dependent (GDD) tuning procedure was developed.[106] In the GDD approach, ω is fine-tuned by using a distance criterion given by $\omega_{\mathrm{GDD}} = C_\omega/\langle d_x\rangle^{-1/2}$. Here, d_x represents the average squared electron-exchange hole distance. The constant C_ω = 0.885 is the value implemented in Q-Chem.[107] To determine the

https://doi.org/10.1021/acs.jctc.4c00005
J. Chem. Theory Comput. 2024, 20, 2520−2537

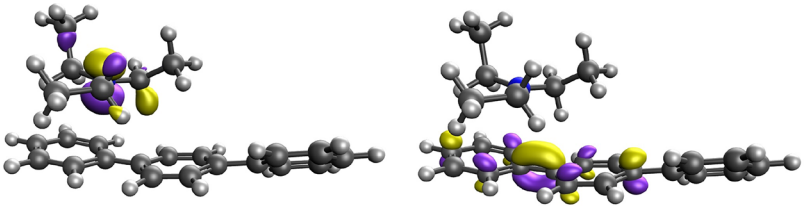

Figure 8. Hole (left) and electron (right) NTOs of [OPP-3−TEA]* exciplex in cyclohexane at the ωPBE/aug-cc-pVDZ level of theory and C-PCM solvent model, chosen based on close agreement with the experimental emission peak (isovalue = 0.2).

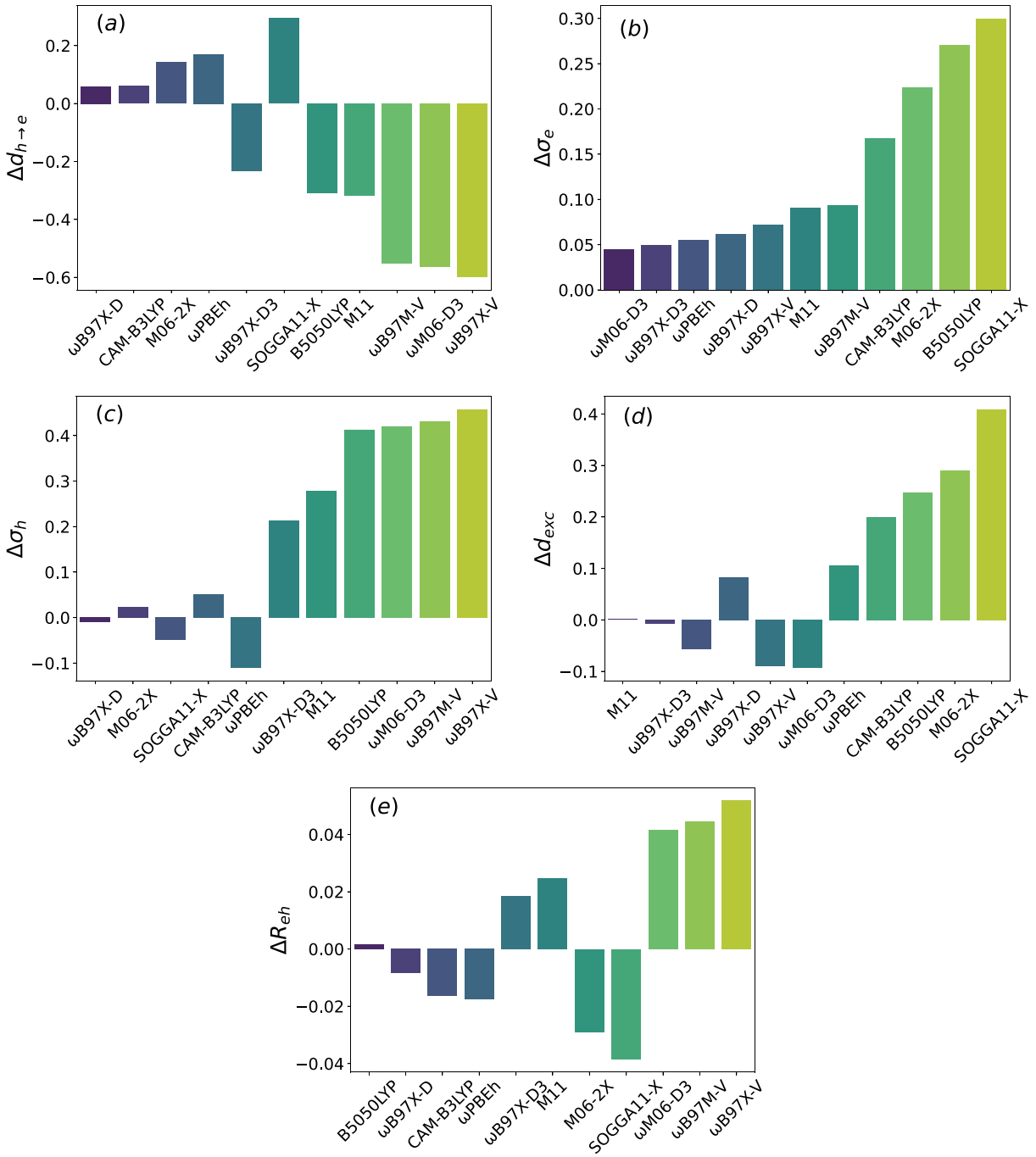

Figure 9. Mean error in exciton properties of [OPP-3−TEA]* exciplexes of different exchange-correlation functionals relative to ωPBE. The exciton descriptors are arranged as (a) average electron−hole distance ($d_{h\to e}$, Å), (b) electron size (σ_e, Å), (c) hole size (σ_h, Å), (d) exciton size (d_{exc}, Å), and (e) correlation coefficient (R_{eh}, dimensionless).

https://doi.org/10.1021/acs.jctc.4c00005
J. Chem. Theory Comput. 2024, 20, 2520−2537

tuned value of the range-separation parameter for two RSH meta-GGAs, ωM06-D3 and ωB97M-V, we first created an optimized ground-state structure of the [OPP-3−TEA] complex. Using this optimized geometry, we then derived the tuned ω_{GDD}. The resulting values are 0.264 for ωM06-D3 and 0.258 for ωB97M-V. This tuning method can, in principle, be applied to all RSH functionals with 100% HF exchange. Our study illustrates the need to regulate the overuse of HF exchange using these two RSH meta-GGAs. Figure 7 shows the emission spectra for [OPP-3−TEA]* exciplexes in CyHex and Et_2O, obtained by using these optimally tuned RSH meta-GGAs.

With the smaller optimally tuned ω values for both ωM06-D3 and ωB97M-V, the resulting spectra are shifted closer to the experiment. In CyHex, the optimally tuned ωM06-D3 and ωB97M-V functional peaks are at 406 and 429 nm, respectively. Notably, the peak obtained from optimally tuned ωB97M-V is the closest to that of the experiment. Whereas the peak from the optimally tuned ωM06-D3 shows improvement over its original counterpart, it remains blue-shifted from the experiment by 22 nm. In the Et_2O solvent, tuning ω shifts the spectra closer to the experiment. However, the peaks for ωM06-D3 and ωB97M-V are blue-shifted from the experiment by 42 and 18 nm, respectively. Although both the original RSHs and the respective optimally tuned counterparts yield reasonable results, it is evident that neither adequately captures the solvatochromic shift. As discussed above and in our previous work,[26] it is evident that implicit models cannot accurately describe the role played by the solvent environment in fluorescence.

Exciton Analysis of Exciplexes. Figure 8 shows the NTOs computed for one of the structures constituting the [OPP-3−TEA]* exciplex ensemble. The hole NTO is localized on TEA, and the electron NTO spans two consecutive phenyl rings of the OPP−3 molecule, which can be described as the $n \rightarrow \pi^*$ CT transition. Tables S9−S13 in the Supporting Information show the exciton properties for [OPP-3−TEA]* exciplexes. As shown in our previous work, the vectorial electron−hole distance ($d_{h\rightarrow e}$) serves as an indicator for the exciplex formation because it quantifies the spatial extent of the CT.[26] In addition to $d_{h\rightarrow e}$, we analyze the electron size, hole size, exciton size, and correlation coefficients. We examine the exciton properties for only those functionals that reliably predict exciplex emission spectra. One meta-GGA, B97M-rV, is also included.

As the exciplex system is too large for EOM-CCSD calculations, we choose ωPBE as the reference based on its accurate prediction of exciplex emission peaks for both OPP-3 and OPP-4. The electron−hole vectorial distance, $d_{h\rightarrow e}$ (Table S9 in the Supporting Information), is larger with the B97M-rV functional. In contrast to ωPBE, the electron NTOs in B97M-rV are more delocalized, spanning all three phenyl rings. This distribution leads to a displacement of the electron NTO centroid, resulting in larger $d_{h\rightarrow e}$ values. Similarly, the increased values of σ_e (Table S10 in the Supporting Information) and d_{exc} (Table S12 in the Supporting Information) are associated with the delocalization of the orbitals and the consequent expansion of NTOs across the entire OPP-3 fragment. As reported in Table S13 of the Supporting Information, most of the R_{eh} values for B97M-rV are negative. This anticorrelation between the hole and the electron suggests that meta-GGA functionals have difficulties describing bound excitons.

Figure 9 presents the mean of deviations of five descriptors, $d_{h\rightarrow e}$, σ_e, σ_h, d_{exc}, and R_{eh}, from the reference ωPBE values. Relative to ωPBE, two RSH GGAs, ωB97X-D3, ωB97X-V, and all considered RSH meta-GGAs functionals yield smaller $d_{h\rightarrow e}$. We find that the functionals with a negative average difference of $d_{h\rightarrow e}$ also have emission peaks at shorter wavelengths than ωPBE. For most exciplexes characterized with ωB97X-D3, ωB97X-V, and RSH meta-GGAs, $d_{h\rightarrow e}$ is shorter than the closest distance between the H atom of TEA and a carbon atom of OPP-3 (2.27 Å on average). This indicates a shift in the centroid of either hole or electron NTOs. Table S9 and Figure 9b indicate that the electron NTO size does not vary much, which implies that $d_{h\rightarrow e}$ is governed by the hole size σ_h.

For the functionals yielding shorter $d_{h\rightarrow e}$ values than those of ωPBE, we find that a small fraction of the hole NTO is present on the OPP-3 fragment. This leads to a larger σ_h (Table S11) and a shift of the centroid of σ_h toward the centroid of σ_e and consequently shorter $d_{h\rightarrow e}$. Other functionals, including SOGGA11-X, M06-2X, and CAM-B3LYP, show larger electron sizes, whereas their hole sizes are comparable to those of the ωPBE values. The exciton sizes [Table S12 and Figure 9d] are also larger for these functionals due to the larger σ_e. All global hybrids, including B5050LYP, show delocalized electron NTOs, underscoring the importance of the correct asymptotic behavior of the exchange potential. The exciton sizes for the RSH meta-GGA functionals are within 0.1 Å of ωPBE.

Table S13 shows that all considered hybrid functionals yield positive correlation coefficients. The condition $R_{eh} > 0$ implies that the electron and hole are bound and move in a correlated way. The functionals with longer emission wavelength than ωPBE, including SOGGA11-X, M06-2X, CAM-B3LYP, ωB97X-D, and ωPBEh, report lower magnitudes of R_{eh}. Similarly, the functionals with a shorter emission wavelength than ωPBE—B5050LYP, ωB97X-D3, ωB97X-V, and all considered RSH meta-GGAs—yield stronger R_{eh} relative to ωPBE. Figure S5 of the Supporting Information shows the average difference in the exciton properties of [OPP-4−TEA]* exciplexes. Functional trends relative to ωPBE for [OPP-4−TEA]* are found to be similar to those for the [OPP-3−TEA]* exciplex.

To understand the extent of CT in different exciplexes as computed by various density functionals, Table S14 in the Supporting Information reports the charge on the TEA fragment. Given the absence of experimental or high-level theoretical reference values, we limit our analysis to observing trends in CT across different density functionals. The minimum, maximum, and mean values of CT are listed in the last three rows of the table. Notably, the B97M-rV meta-GGA functional demonstrates a significant extent of CT, occasionally indicating complete CT, which is not characteristic of exciplex behavior and is thus deemed inaccurate. On the other hand, RSH meta-GGAs tend to yield lower values of CT. Among global hybrid functionals, those with a higher fraction of HF exchange generally exhibit reduced CT. Given the satisfactory performance of the ωPBE functional in predicting other properties, we consider other RSH GGAs that yield results similar to ωPBE to be more accurate in their treatment of CT.

Although three global hybrid functionals—B5050LYP, SOGGA11-X, and M06-2X—yield reasonably accurate emission spectra, the electron size is larger because of delocalization spreading to the third phenyl ring. Overall, the B5050LYP and M06-2X functionals are more reliable among all global hybrids due to the improved treatment of the Coulomb interaction. In addition to ωPBE, RSH functionals CAM-B3LYP and ωB97X-D reliably describe both emission energies and exciton properties. However, the RSH meta-GGAs are not recommended for excited-state CT complexes due to their tendency to

https://doi.org/10.1021/acs.jctc.4c00005
J. Chem. Theory Comput. 2024, 20, 2520−2537

overestimate emission energies and the inadequate treatment of hole NTOs.

By analyzing the emission energies of isolated chromophores and the emission spectra of the corresponding exciplexes and their excitons, we observe that meta-GGA functionals fail to reproduce experimental emission energies. Meta-GGA functionals also fail to produce physically correct exciton descriptors. The performance of global hybrid functionals largely depends on the percentage of exact exchange included in their formulation. The global hybrid GGA functional B5050LYP (50% HF exchange) and the global hybrid meta-GGA functional M06-2X (54% HF exchange) are observed to be the best for emission properties. However, they tend to yield more delocalized excitons. Among all density functionals, the RSH GGAs are the most accurate, with ωPBE and ωB97X-D being the most reliable. ωPBEh, ωB97X-V, and ωB97X-D3 also reasonably describe the emission energies and exciton properties of isolated chromophores. Due to the overestimation of emission energies, RSH meta-GGAs are not recommended for emission spectra calculations. To summarize, the main recommendation emerging from this benchmarking study is that RSH GGAs are suitable for studying fluorescence of both organic chromophores and their intermolecular CT exciplexes. Study of the latter requires the correct description of the exciplex state, and our method to generate an ensemble of structures is one such viable approach.

CONCLUSIONS

We report a comprehensive examination of the emission spectra and excited-state properties of isolated organic chromophores, OPP-N (N = 3, 4), and their exciplexes with TEA using a large set of exchange-correlation functionals. We probed the accuracies of meta-GGAs, global hybrids, and RSHs. The exciplex state was represented using an ensemble of geometries with distinct electronic and emission energies that together yield the broad, red-shifted emission peak that is observed in the experiments. The protocol for TDDFT optimization and verification of the distribution of geometries constituting the exciplex state is identical to our previous work.[26] The solvatochromic shifts of both isolated chromophores and exciplexes were analyzed by calculating their emission energies in various solvents. We also computed the exciton properties, including the electron−hole distance, the exciton size, the electron size, the hole size, and the electron−hole correlation coefficient. The results obtained with DFT were benchmarked against experimental emission energies and, when feasible, against the EOM-CCSD method.

Meta-GGA functionals tend to underestimate the isolated chromophores' and exciplex emission energies significantly compared to experimental values. They fail to adequately describe the bound state of the electron−hole pair for both isolated chromophores and exciplexes. The computed hole and electron sizes by meta-GGA are also relatively larger compared to those of other functionals. In global hybrids, both the emission energy and exciton descriptors are strongly influenced by the fraction of the exact exchange. Notably, the TPSSh hybrid functional, which includes only 10% of HF exchange, yields the least accurate emission energies and is the only hybrid functional that predicts an anticorrelated electron−hole pair. On the other hand, the SOGGA11-X, B5050LYP, and M06-2X functionals, containing HF percentages of 40.15, 50, and 54, respectively, demonstrate good agreement in emission energies and exciton descriptors when compared with experimental data and EOM-CCSD. Of the functionals examined, RSH GGAs stand out as reasonably effective for analyzing emission properties. On average, ωPBE emerges as the most accurate functional for computing emission energies and exciton descriptors of isolated chromophores and exciplexes, as well as for determining the shift in the emission peak from [OPP-3−TEA]* to [OPP-4−TEA]* exciplexes. Additionally, CAM-B3LYP, ωPBEH, and ωB97X-D are identified as the next best options for emission studies.

RSH meta-GGAs, specifically M11, ωM06-D3, and ωB97M-V, yield results comparable to those of RSH GGAs in terms of emission energies and exciton properties for isolated chromophores. However, their application to exciplexes yields unsatisfactory results, with all three functionals significantly overestimating the emission energies. This motivated us to adjust the range-separation parameter (ω) using the GDD tuning procedure. With optimized ω, there is noticeable improvement in emission energies, bringing the emission spectra much closer to experimental values. Therefore, we recommend reoptimizing the ω parameter for specific systems when using RSH meta-GGA functionals. In summary, our study provides benchmark results for popular density functionals for computing emission properties in isolated chromophores and exciplexes. The analysis of the exciton descriptors provides new insights into the performance of various functionals.

ASSOCIATED CONTENT

Data Availability Statement

The data supporting this study's findings are available within the article and its Supporting Information file. The exciplex geometries are available in the manuscript.

Supporting Information

The Supporting Information is available free of charge at https://pubs.acs.org/doi/10.1021/acs.jctc.4c00005.

The optimized data for all isolated chromophores and exciplexes are hosted on Zenodo (ZIP)[108]

Emission energies for [OPP-4]* and emission spectra of [OPP-4−TEA]* exciplexes and all data describing exciton descriptors (PDF)

AUTHOR INFORMATION

Corresponding Authors

Anna I. Krylov − *Department of Chemistry, University of Southern California, Los Angeles, California 90089, United States;* orcid.org/0000-0001-6788-5016; Email: krylov@usc.edu

Shaama Mallikarjun Sharada − *Mork Family Department of Chemical Engineering and Materials Science and Department of Chemistry, University of Southern California, Los Angeles, California 90089, United States;* orcid.org/0000-0001-7332-5373; Email: ssharada@usc.edu

Authors

Abhilash Patra − *Mork Family Department of Chemical Engineering and Materials Science, University of Southern California, Los Angeles, California 90089, United States;* orcid.org/0000-0001-5792-3875

George Baffour Pipim − *Department of Chemistry, University of Southern California, Los Angeles, California 90089, United States;* orcid.org/0000-0002-4700-8005

Complete contact information is available at: https://pubs.acs.org/10.1021/acs.jctc.4c00005

https://doi.org/10.1021/acs.jctc.4c00005
J. Chem. Theory Comput. 2024, 20, 2520−2537

Author Contributions

[§]A.P. and G.B.P. contributed equally to this work.

Notes

The authors declare the following competing financial interest(s): A.I.K. is the president and a part-owner of Q-Chem, Inc.

■ ACKNOWLEDGMENTS

This work is supported by the U.S. Department of Energy, Office of Science, Office of Basic Energy Sciences under award number DE-SC0022326. The authors also acknowledge the computational resources and support from the USC's Center for Advanced Research Computing (CARC) and the National Energy Research Scientific Computing Center (NERSC). The authors are grateful to Prof. Jahan Dawlaty and Mr. Goran Giudetti for helpful discussions.

■ REFERENCES

(1) Hohenberg, P.; Kohn, W. Inhomogeneous electron gas. *Phys. Rev.* **1964**, *136*, B864−B871.
(2) Kohn, W.; Sham, L. J. Self-consistent equations including exchange and correlation effects. *Phys. Rev.* **1965**, *140*, A1133−A1138.
(3) Runge, E.; Gross, E. K. U. Density-functional theory for time-dependent systems. *Phys. Rev. Lett.* **1984**, *52*, 997−1000.
(4) Casida, M. E. Time-dependent density functional response theory for molecules; *Recent Advances in Computational Chemistry*; World Scientific, 1995; *1*; 155−192.
(5) Teale, A.; et al. DFT exchange: Sharing perspectives on the workhorse of quantum chemistry and materials science. *Phys. Chem. Chem. Phys.* **2022**, *24*, 28700−28781.
(6) Dreuw, A.; Head-Gordon, M. Single-reference ab initio methods for the calculation of excited states of large molecules. *Chem. Rev.* **2005**, *105*, 4009−4037.
(7) Mardirossian, N.; Head-Gordon, M. Thirty years of density functional theory in computational chemistry: An overview and extenive assessment of 200 density functionals. *Mol. Phys.* **2017**, *115*, 2315−2372.
(8) Jacquemin, D.; Perpète, E. A.; Vydrov, O. A.; Scuseria, G. E.; Adamo, C. Assessment of long-range corrected functionals performance for n→π^* transitions in organic dyes. *J. Chem. Phys.* **2007**, *127*, No. 094102.
(9) Jacquemin, D.; Wathelet, V.; Perpete, E. A.; Adamo, C. Extensive TD-DFT benchmark: singlet-excited states of organic molecules. *J. Chem. Theory Comput.* **2009**, *5*, 2420−2435.
(10) Silverstein, D. W.; Jensen, L. Assessment of the accuracy of long-range corrected functionals for describing the electronic and optical properties of silver clusters. *J. Chem. Phys.* **2010**, *132*, 194302.
(11) Jacquemin, D.; Perpete, E. A.; Ciofini, I.; Adamo, C.; Valero, R.; Zhao, Y.; Truhlar, D. G. On the performances of the M06 family of density functionals for electronic excitation energies. *J. Chem. Theory Comput.* **2010**, *6*, 2071−2085.
(12) Jacquemin, D.; Mennucci, B.; Adamo, C. Excited-state calculations with TD-DFT: from benchmarks to simulations in complex environments. *Phys. Chem. Chem. Phys.* **2011**, *13*, 16987−16998.
(13) Peverati, R.; Truhlar, D. G. Performance of the M11 and M11-L density functionals for calculations of electronic excitation energies by adiabatic time-dependent density functional theory. *Phys. Chem. Chem. Phys.* **2012**, *14*, 11363−11370.
(14) Lin, Y.-S.; Tsai, C.-W.; Li, G.-D.; Chai, J.-D. Long-range corrected hybrid meta-generalized-gradient approximations with dispersion corrections. *J. Chem. Phys.* **2012**, *136*, 154109.
(15) Leang, S. S.; Zahariev, F.; Gordon, M. S. Benchmarking the performance of time-dependent density functional methods. *J. Chem. Phys.* **2012**, *136*, 104101.
(16) Shao, Y.; Mei, Y.; Sundholm, D.; Kaila, V. R. I. Benchmarking the performance of time-dependent density functional theory methods on biochromophores. *J. Chem. Theory Comput.* **2020**, *16*, 587−600.
(17) Shu, Y.; Truhlar, D. G. Relationships between orbital energies, optical and fundamental gaps, and exciton shifts in approximate density functional theory and quasiparticle theory. *J. Chem. Theory Comput.* **2020**, *16*, 4337−4350.
(18) Jacquemin, D. What is the key for accurate absorption and emission calculations, energy or geometry? *J. Chem. Theory Comput.* **2018**, *14*, 1534−1543.
(19) Mewes, S. A.; Plasser, F.; Krylov, A.; Dreuw, A. Benchmarking excited-state calculations using exciton properties. *J. Chem. Theory Comput.* **2018**, *14*, 710−725.
(20) Matsuoka, S.; Kohzuki, T.; Pac, C.; Ishida, A.; Takamuku, S.; Kusaba, M.; Nakashima, N.; Yanagida, S. Photocatalysis of oligo (p-phenylenes): Photochemical reduction of carbon dioxide with triethylamine. *J. Phys. Chem.* **1992**, *96*, 4437−4442.
(21) Seo, H.; Liu, A.; Jamison, T. F. Direct β-selective hydrocarboxylation of styrenes with CO_2 enabled by continuous flow photoredox catalysis. *J. Am. Chem. Soc.* **2017**, *139*, 13969−13972.
(22) Seo, H.; Katcher, M. H.; Jamison, T. F. Photoredox activation of carbon dioxide for amino acid synthesis in continuous flow. *Nat. Chem.* **2017**, *9*, 453.
(23) Kron, K. J.; Hunt, J. R.; Dawlaty, J. M.; Mallikarjun Sharada, S. Modeling and characterization of exciplexes in photoredox CO_2 reduction: Insights from quantum chemistry and fluorescence spectroscopy. *J. Phys. Chem. A* **2022**, *126*, 2319−2329.
(24) Stanton, J. F.; Bartlett, R. J. The equation of motion coupled-cluster method. A systematic biorthogonal approach to molecular excitation energies, transition probabilities, and excited state properties. *J. Chem. Phys.* **1993**, *98*, 7029−7039.
(25) Krylov, A. I. Equation-of-motion coupled-cluster methods for open-shell and electronically excited species: The hitchhiker's guide to Fock space. *Annu. Rev. Phys. Chem.* **2008**, *59*, 433−462.
(26) Patra, A.; Krylov, A. I.; Mallikarjun Sharada, S. Simulating excited-state complex ensembles: Fluorescence and solvatochromism in amine-arene exciplexes. *J. Chem. Phys.* **2023**, *159*, No. 064101.
(27) Plasser, F.; Krylov, A. I.; Dreuw, A. libwfa: Wavefunction analysis tools for excited and open-shell electronic states. *WIREs: Comput. Mol. Sci.* **2022**, *12*, No. e1595.
(28) Luzanov, A. V.; Sukhorukov, A. A.; Umanskii, V. E. Application of transition density matrix for analysis of excited states. *Theor. Exp. Chem.* **1976**, *10*, 354−361. Russian original: Teor. *Eksp. Khim.*, **1974** *10*, 456.
(29) Luzanov, A. V.; Pedash, V. F. Interpretation of excited states using charge-transfer number. *Theor. Exp. Chem.* **1980**, *15*, 338−341.
(30) Head-Gordon, M.; Grana, A. M.; Maurice, D.; White, C. A. Analysis of electronic transitions as the difference of electron attachment and detachment densities. *J. Phys. Chem.* **1995**, *99*, 14261−14270.
(31) Martin, R. L. Natural transition orbitals. *J. Phys. Chem. A* **2003**, *118*, 4775−4777.
(32) Mayer, I. Using singular value decomposition for a compact presentation and improved interpretation of the CIS wave functions. *Chem. Phys. Lett.* **2007**, *437*, 284−286.
(33) Surján, P. R. Natural orbitals in CIS and singular-value decomposition. *Chem. Phys. Lett.* **2007**, *439*, 393−394.
(34) Plasser, F.; Wormit, M.; Dreuw, A. New tools for the systematic analysis and visualization of electronic excitations. I. Formalism. *J. Chem. Phys.* **2014**, *141*, No. 024106.
(35) Plasser, F.; Bäppler, S. A.; Wormit, M.; Dreuw, A. New tools for the systematic analysis and visualization of electronic excitations II. Applications. *J. Chem. Phys.* **2014**, *141*, No. 024107.
(36) Bäppler, S. A.; Plasser, F.; Wormit, M.; Dreuw, A. Exciton analysis of many-body wave functions: Bridging the gap between the quasiparticle and molecular orbital pictures. *Phys. Rev. A* **2014**, *90*, No. 052521.
(37) Kimber, P.; Plasser, F. Toward an understanding of electronic excitation energies beyond the molecular orbital picture. *Phys. Chem. Chem. Phys.* **2020**, *22*, 6058−6080.

https://doi.org/10.1021/acs.jctc.4c00005
J. Chem. Theory Comput. 2024, 20, 2520−2537

(38) Improta, R.; Scalmani, G.; Frisch, M. J.; Barone, V. Toward effective and reliable fluorescence energies in solution by a new state specific polarizable continuum model time dependent density functional theory approach. *J. Chem. Phys.* **2007**, *127*, No. 074504.
(39) Kümmel, S. Charge-transfer excitations: A challenge for time-dependent density functional theory that has been met. *Adv. Energy Mater.* **2017**, *7*, 1700440.
(40) Perdew, J. P.; Schmidt, K. Jacob's ladder of density functional approximations for the exchange-correlation energy. *AIP Conf. Proc.* **2001**, *577*, 1−20.
(41) Zhao, Y.; Truhlar, D. G. A new local density functional for main-group thermochemistry, transition metal bonding, thermochemical kinetics, and noncovalent interactions. *J. Chem. Phys.* **2006**, *125*, 194101.
(42) Wang, Y.; Jin, X.; Yu, H. S.; Truhlar, D. G.; He, X. Revised M06-L functional for improved accuracy on chemical reaction barrier heights, noncovalent interactions, and solid-state physics. *Proc. Natl. Acad. Sci. U. S. A.* **2017**, *114*, 8487−8492.
(43) Sun, J.; Ruzsinszky, A.; Perdew, J. P. Strongly constrained and appropriately normed semilocal density functional. *Phys. Rev. Lett.* **2015**, *115*, No. 036402.
(44) Furness, J. W.; Kaplan, A. D.; Ning, J.; Perdew, J. P.; Sun, J. Accurate and numerically efficient r^{2}SCAN meta-generalized gradient approximation. *J. Phys. Chem. Lett.* **2020**, *11*, 8208−8215.
(45) Mardirossian, N.; Ruiz Pestana, L.; Womack, J. C.; Skylaris, C.-K.; Head-Gordon, T.; Head-Gordon, M. Use of the rVV10 nonlocal correlation functional in the B97M-V density functional: Defining B97M-rV and related functionals. *J. Phys. Chem. Lett.* **2017**, *8*, 35−40.
(46) Van Voorhis, T.; Scuseria, G. E. A novel form for the exchange-correlation energy functional. *J. Chem. Phys.* **1998**, *109*, 400−410.
(47) Perdew, J. P.; Burke, K.; Ernzerhof, M. Generalized gradient approximation made simple. *Phys. Rev. Lett.* **1996**, *77*, 3865−3868.
(48) Becke, A. D. Density-functional thermochemistry. IV. A new dynamical correlation functional and implications for exact-exchange mixing. *J. Chem. Phys.* **1996**, *104*, 1040−1046.
(49) Bartók, A. P.; Yates, J. R. Regularized SCAN functional. *J. Chem. Phys.* **2019**, *150*, 161101.
(50) Jana, S.; Patra, A.; Samal, P. Assessing the performance of the Tao-Mo semilocal density functional in the projector-augmented-wave method. *J. Chem. Phys.* **2018**, *149*, No. 044120.
(51) Kingsbury, R.; Gupta, A. S.; Bartel, C. J.; Munro, J. M.; Dwaraknath, S.; Horton, M.; Persson, K. A. Performance comparison of *r*^{2}SCANand SCAN metaGGA density functionals for solid materials via an automated, high-throughput computational workflow. *Phys. Rev. Mater.* **2022**, *6*, No. 013801.
(52) Kothakonda, M.; Kaplan, A. D.; Isaacs, E. B.; Bartel, C. J.; Furness, J. W.; Ning, J.; Wolverton, C.; Perdew, J. P.; Sun, J. Testing the r^{2}SCAN density functional for the thermodynamic stability of solids with and without a van der Waals correction. *ACS Materials Au* **2023**, *3*, 102−111.
(53) Becke, A. D. Density-functional thermochemistry. V. Systematic optimization of exchange-correlation functionals. *J. Chem. Phys.* **1997**, *107*, 8554−8560.
(54) Sabatini, R.; Gorni, T.; de Gironcoli, S. Nonlocal van der Waals density functional made simple and efficient. *Phys. Rev. B* **2013**, *87*, No. 041108.
(55) Stephens, P. J.; Devlin, F. J.; Chabalowski, C. F.; Frisch, M. J. Ab initio calculation of vibrational absorption and circular dichroism spectra using density functional force fields. *J. Phys. Chem.* **1994**, *98*, 11623−11627.
(56) Adamo, C.; Barone, V. Toward reliable density functional methods without adjustable parameters: The PBE0 model. *J. Chem. Phys.* **1999**, *110*, 6158−6170.
(57) Ernzerhof, M.; Scuseria, G. E. Assessment of the Perdew−Burke−Ernzerhof exchange-correlation functional. *J. Chem. Phys.* **1999**, *110*, 5029−5036.
(58) Shao, Y.; Head-Gordon, M.; Krylov, A. I. The spin−flip approach within time-dependent density functional theory: Theory and applications to diradicals. *J. Chem. Phys.* **2003**, *118*, 4807−4818.
(59) Peverati, R.; Truhlar, D. G. Communication: A global hybrid generalized gradient approximation to the exchange-correlation functional that satisfies the second-order density-gradient constraint and has broad applicability in chemistry. *J. Chem. Phys.* **2011**, *135*, 191102.
(60) Staroverov, V. N.; Scuseria, G. E.; Tao, J.; Perdew, J. P. Comparative assessment of a new nonempirical density functional: Molecules and hydrogen-bonded complexes. *J. Chem. Phys.* **2003**, *119*, 12129−12137.
(61) Zhao, Y.; Truhlar, D. G. The M06 suite of density functionals for main group thermochemistry, thermochemical kinetics, noncovalent interactions, excited states, and transition elements: two new functionals and systematic testing of four M06-class functionals and 12 other functionals. *Theor. Chem. Acc.* **2008**, *120*, 215−241.
(62) Hui, K.; Chai, J. D. SCAN-based hybrid and double-hybrid density functionals from models without fitted parameters. *J. Chem. Phys.* **2016**, *144*, No. 044114.
(63) Gill, P. M. W.; Johnson, B. G.; Pople, J. A.; Frisch, M. J. An investigation of the performance of a hybrid of Hartree-Fock and density functional theory. *Int. J. Quantum Chem.* **1992**, *44*, 319−331.
(64) Perdew, J. P.; Ernzerhof, M.; Burke, K. Rationale for mixing exact exchange with density functional approximations. *J. Chem. Phys.* **1996**, *105*, 9982−9985.
(65) Ruzsinszky, A.; Perdew, J. P.; Csonka, G. I.; Vydrov, O. A.; Scuseria, G. E. Spurious fractional charge on dissociated atoms: Pervasive and resilient self-interaction error of common density functionals. *J. Chem. Phys.* **2006**, *125*, 194112.
(66) Schmidt, T.; Kümmel, S. One- and many-electron self-interaction error in local and global hybrid functionals. *Phys. Rev. B* **2016**, *93*, 165120.
(67) Bryenton, K. R.; Adeleke, A. A.; Dale, S. G.; Johnson, E. R. Delocalization error: The greatest outstanding challenge in density-functional theory. *WIREs Comput. Mol. Sci.* **2023**, *13*, No. e1631.
(68) Yanai, T.; Tew, D. P.; Handy, N. C. A new hybrid exchange−correlation functional using the Coulomb-attenuating method (CAM-B3LYP). *Chem. Phys. Lett.* **2004**, *393*, 51−57.
(69) Henderson, T. M.; Janesko, B. G.; Scuseria, G. E. Generalized gradient approximation model exchange holes for range-separated hybrids. *J. Chem. Phys.* **2008**, *128*, 194105.
(70) Rohrdanz, M. A.; Herbert, J. M. Simultaneous benchmarking of ground- and excited-state properties with long-range-corrected density functional theory. *J. Chem. Phys.* **2008**, *129*, No. 034107.
(71) Chai, J.-D.; Head-Gordon, M. Long-range corrected hybrid density functionals with damped atom−atom dispersion corrections. *Phys. Chem. Chem. Phys.* **2008**, *10*, 6615−6620.
(72) Rohrdanz, M. A.; Martins, K. M.; Herbert, J. M. A long-range-corrected density functional that performs well for both ground-state properties and time-dependent density functional theory excitation energies, including charge-transfer excited states. *J. Chem. Phys.* **2009**, *130*, No. 054112.
(73) Lin, Y.-S.; Li, G.-D.; Mao, S.-P.; Chai, J.-D. Long-range corrected hybrid density functionals with improved dispersion corrections. *J. Chem. Theory Comput.* **2013**, *9*, 263−272.
(74) Mardirossian, N.; Head-Gordon, M. B97X-V: A 10-parameter, range-separated hybrid, generalized gradient approximation density functional with nonlocal correlation, designed by a survival-of-the-fittest strategy. *Phys. Chem. Chem. Phys.* **2014**, *16*, 9904−9924.
(75) Peverati, R.; Truhlar, D. G. Improving the accuracy of hybrid meta-GGA density functionals by range separation. *J. Phys. Chem. Lett.* **2011**, *2*, 2810−2817.
(76) Mardirossian, N.; Head-Gordon, M. Mapping the genome of meta-generalized gradient approximation density functionals: The search for B97M-V. *J. Chem. Phys.* **2015**, *142*, No. 074111.
(77) Champagne, B.; Perpéte, E. A.; van Gisbergen, S. J. A.; Baerends, E.-J.; Snijders, J. G.; Soubra-Ghaoui, C.; Robins, K. A.; Kirtman, B. Assessment of conventional density functional schemes for computing the polarizabilities and hyperpolarizabilities of conjugated oligomers: An ab initio investigation of polyacetylene chains. *J. Chem. Phys.* **1998**, *109*, 10489−10498.

https://doi.org/10.1021/acs.jctc.4c00005
J. Chem. Theory Comput. 2024, 20, 2520−2537

(78) Dreuw, A.; Weisman, J. L.; Head-Gordon, M. Long-range charge-transfer excited states in time-dependent density functional theory require non-local exchange. *J. Chem. Phys.* **2003**, *119*, 2943−2946.
(79) Weintraub, E.; Henderson, T. M.; Scuseria, G. E. Long-range-corrected hybrids based on a new model exchange hole. *J. Chem. Theory Comput.* **2009**, *5*, 754−762.
(80) Jana, S.; Patra, A.; Constantin, L. A.; Myneni, H.; Samal, P. Long-range screened hybrid-functional theory satisfying the local-density linear response. *Phys. Rev. A* **2019**, *99*, No. 042515.
(81) Verma, P.; Bartlett, R. J. Increasing the applicability of density functional theory. IV. Consequences of ionization-potential improved exchange-correlation potentials. *J. Chem. Phys.* **2014**, *140*, 18A534.
(82) Jin, Y.; Bartlett, R. J. The QTP family of consistent functionals and potentials in Kohn-Sham density functional theory. *J. Chem. Phys.* **2016**, *145*, No. 034107.
(83) Jacquemin, D.; Perpéte, E. A.; Scalmani, G.; Frisch, M. J.; Kobayashi, R.; Adamo, C. Assessment of the efficiency of long-range corrected functionals for some properties of large compounds. *J. Chem. Phys.* **2007**, *126*, 144105.
(84) Liang, J.; Feng, X.; Hait, D.; Head-Gordon, M. Revisiting the performance of time-dependent density functional theory for electronic excitations: Assessment of 43 popular and recently developed functionals from rungs one to four. *J. Chem. Theory Comput.* **2022**, *18*, 3460−3473.
(85) Jacquemin, D.; Perpéte, E. A.; Scuseria, G. E.; Ciofini, I.; Adamo, C. TD-DFT performance for the visible absorption spectra of organic dyes: Conventional versus long-range hybrids. *J. Chem. Theory Comput.* **2008**, *4*, 123−135.
(86) da Silva, P. S. P.; Martiın-Ramos, P.; Domingos, S. R.; Bota de Sousa, M. D. C.; Arranja, C. T.; Sobral, A. J. F. N.; Ramos Silva, M. On the performance of hybrid functionals for non-linear optical properties and electronic excitations in chiral molecular rystals: The case of butterfly-shaped dicinnamalacetone. *ChemPhysChem* **2018**, *19*, 82−92.
(87) Plasser, F.; Bäppler, S. A.; Wormit, M.; Dreuw, A. New tools for the systematic analysis and visualization of electronic excitations. II. Applications. *J. Chem. Phys.* **2014**, *141*, 024107 DOI: 10.1063/1.4885820.
(88) Mayer, I. Using singular value decomposition for a compact presentation and improved interpretation of the CIS wave functions. *Chemical physics letters* **2007**, *437*, 284−286.
(89) Epifanovsky, E.; Gilbert, A. T. B.; Feng, X.; Lee, J.; Mao, Y.; Mardirossian, N.; Pokhilko, P.; White, A. F.; Coons, M. P.; Dempwolff, A. L.; et al. Software for the frontiers of quantum chemistry: An overview of developments in the Q-Chem 5 package. *J. Chem. Phys.* **2021**, *155*, No. 084801.
(90) Barone, V.; Cossi, M. Quantum calculation of molecular energies and energy gradients in solution by a conductor solvent model. *J. Phys. Chem. A* **1998**, *102*, 1995−2001.
(91) Cossi, M.; Rega, N.; Scalmani, G.; Barone, V. Energies, structures, and electronic properties of molecules in solution with the C-PCM solvation model. *J. Comput. Chem.* **2003**, *24*, 669−681.
(92) Marenich, A. V.; Cramer, C. J.; Truhlar, D. G. Universal solvation model based on solute electron density and on a continuum model of the solvent defined by the bulk dielectric constant and atomic surface tensions. *J. Phys. Chem. B* **2009**, *113*, 6378−6396.
(93) Cammi, R.; Tomasi, J. Nonequilibrium solvation theory for the polarizable continuum model: A new formulation at the SCF level with application to the case of the frequency-dependent linear electric response function. *Int. J. Quantum Chem.* **1995**, *56*, 465−474.
(94) Cossi, M.; Barone, V. Separation between fast and slow polarizations in continuum solvation models. *J. Phys. Chem. A* **2000**, *104*, 10614−10622.
(95) Improta, R.; Barone, V.; Scalmani, G.; Frisch, M. J. A state-specific polarizable continuum model time dependent density functional theory method for excited state calculations in solution. *J. Chem. Phys.* **2006**, *125*, No. 054103.
(96) You, Z.-Q.; Mewes, J.-M.; Dreuw, A.; Herbert, J. M. Comparison of the Marcus and Pekar partitions in the context of non-equilibrium, polarizable-continuum solvation models. *J. Chem. Phys.* **2015**, *143*, 204104.
(97) Ge, Q.; Mao, Y.; Head-Gordon, M. Energy decomposition analysis for exciplexes using absolutely localized molecular orbitals. *J. Chem. Phys.* **2018**, *148*, No. 064105.
(98) Ge, Q.; Head-Gordon, M. Energy decomposition analysis for excimers using absolutely localized molecular orbitals within time-dependent density functional theory and configuration interaction with single excitations. *J. Chem. Theory Comput.* **2018**, *14*, 5156−5168.
(99) Krylov, A. I. From orbitals to observables and back. *J. Chem. Phys.* **2020**, *153*, No. 080901.
(100) Cardeynaels, T.; Paredis, S.; Deckers, J.; Brebels, S.; Vanderzande, D.; Maes, W.; Champagne, B. Finding the optimal exchange−correlation functional to describe the excited state properties of push−pull organic dyes designed for thermally activated delayed fluorescence. *Phys. Chem. Chem. Phys.* **2020**, *22*, 16387−16399.
(101) Véril, M.; Scemama, A.; Caffarel, M.; Lipparini, F.; Boggio-Pasqua, M.; Jacquemin, D.; Loos, P. QUESTDB: A database of highly accurate excitation energies for the electronic structure community. *WIREs Comput. Mol. Sci.* **2021**, *11*, No. e1517.
(102) Körzdöfer, T.; Brédas, J.-L. Organic electronic materials: Recent advances in the DFT description of the ground and excited states using tuned range-separated hybrid functionals. *Acc. Chem. Res.* **2014**, *47*, 3284−3291.
(103) Baer, R.; Livshits, E.; Salzner, U. Tuned range-Sseparated hybrids in density functional theory. *Annu. Rev. Phys. Chem.* **2010**, *61*, 85−109.
(104) Körzdöfer, T.; Sears, J. S.; Sutton, C.; Brédas, J.-L. Long-range corrected hybrid functionals for π-conjugated systems: Dependence of the range-separation parameter on conjugation length. *J. Chem. Phys.* **2011**, *135*, 204107.
(105) Karolewski, A.; Kronik, L.; Kümmel, S. Using optimally tuned range separated hybrid functionals in ground-state calculations: Consequences and caveats. *J. Chem. Phys.* **2013**, *138*, 204115.
(106) Modrzejewski, M.; Rajchel; Chalasinski, G.; Szczesniak, M. M. Density-dependent onset of the long-range exchange: A key to donor−acceptor properties. *J. Phys. Chem. A* **2013**, *117*, 11580−11586.
(107) Lao, K. U.; Herbert, J. M. Atomic orbital implementation of extended symmetry-adapted perturbation theory (XSAPT) and benchmark calculations for large supramolecular complexes. *J. Chem. Theory Comput.* **2018**, *14*, 2955−2978.
(108) Patra, A.; Baffour Pipim, G.; Krylov, A.; Mallikarjun Sharada, S. Supporting data set for "Performance of density functionals for excited-state properties of isolated chromophores and exciplexes: Emission spectra, solvatochromic shifts, and charge- transfer character. 2024, DOI: 10.5281/zenodo.10712418.